Journal of Mathematical Chemistry Vol. 35, No. 3, March 2004 (© 2004)

General-model-space state–universal coupled-cluster method: Diagrammatic approach

Josef Paldus*,[1], Xiangzhu Li and Nicholas D.K. Petraco

Also at: Department of Applied Mathematics, University of Waterloo, Waterloo, Ontario, Canada N2L 3G1
E-mail: paldus@theochem.uwaterloo.ca

Received 10 December 2003; revised 11 March 2004

The explicit expressions for the recently formulated general-model-space (GMS) version of the multireference state-universal (SU) coupled-cluster (CC) method [X. Li and J. Paldus, J. Chem. Phys. 119 (2003) 5320], truncated at the level of single (S) and double (D) excitations, are re-derived using the spin-orbital form of the diagrammatic technique. The focus is on the so-called coupling coefficients, which represent a new type of quantity that does not appear in the single-reference CC approaches. The role of the connectivity conditions, referred to as the C-conditions, in the elimination of disconnected terms in the GMS SU CC method is analyzed in terms of the connectivity of the resulting diagrams and is illustrated on typical examples.

KEY WORDS: multireference state-universal coupled-cluster method, general model space, complete model space, diagrammatic technique

AMS subject classification: 81G45, 81G55, 81C30, 81H99, 94C15

1. Introduction

The multi reference (MR) generalizations of the standard single reference (SR) coupled-cluster (CC) method are invariably based on the effective Hamiltonian formalism (see, e.g., [1–3]). The effective Hamiltonian $H^{(\mathrm{eff})}$ is defined on a suitably chosen, finite-dimensional model space $\mathcal{M}_0$, $\mathcal{M}_0 = \mathrm{Span}\{|\Phi_i\rangle : i = 1, \ldots, M\}$, via the wave operator U which, in turn, is determined by the generalized Bloch equation. With a suitable choice of the model space $\mathcal{M}_0$ this formalism yields, in principle, the exact solution of the respective Schrödinger equation, equation (1), for a finite number M of target states $|\Psi_i\rangle$,

$$H|\Psi_i\rangle = E_i|\Psi_i\rangle\,. \tag{1}$$

* Corresponding author.
[1] Also at: Department of Chemistry, and Guelph-Waterloo Center for Graduate Work in Chemistry – Waterloo Campus, University of Waterloo, Waterloo, Ontario, Canada N2L 3G1.

0259-9791/04/0300-0215/0

The crucial step in the design of the MR version of the CC theory that is based on the effective Hamiltonian formalism is the generalization of the SR CC Ansatz. Unfortunately, such a generalization is not unambiguous and, currently, two distinct formulations are available, leading to the so-called *valence universal* (VU) or *Fock space* [4–8] and *state-universal* (SU) or *Hilbert space* [9] methods. The VU approach is characterized by the cluster Ansatz involving a single-cluster operator. However, this Ansatz necessitates the consideration of an entire chain of model spaces that involve a varying number of electrons (see, e.g., [8]). In contrast, the SU approach employs one and only one model space, characterized by a fixed number of valence electrons, and associates a distinct cluster operator $T(i)$ with each reference configuration $|\Phi_i\rangle$, so that

$$U = \sum_{i=1}^{M} e^{T(i)} |\Phi_i\rangle\langle\Phi_i| \,. \tag{2}$$

In this paper we focus solely on the SU CC approach.

Although both genuine MR CC approaches just mentioned were formulated more than two decades ago, only a few applications to actual systems have been made in the meantime and no generic codes have been developed. One of the reasons for the lack of practical exploitations of these methods is undoubtedly the fact that in their standard version they suffer from several impediments, not to mention their complexity and computational demands. Perhaps the most serious obstacle in actual applications to the molecular electronic structure is the so-called *intruder state problem*. Just as in the SR case, where the reference configuration $|\Phi_0\rangle$ is required to be nondegenerate [10,11] and to provide a reasonable approximation to the ground state wave function $|\Psi\rangle$, the choice of the model space $\mathcal{M}_0$ should be such that its spanning set $\{|\Phi_i\rangle : i = 1, \ldots, M\}$ is not quasidegenerate with other configurations belonging to the same symmetry species and that each target wave function $|\Psi_i\rangle$ has a sizeable component within $\mathcal{M}_0$. While this requirement can be reasonably satisfied at one, say equilibrium, geometry, this may no longer be the case at another geometry, since the manifold of excited state potential energy surfaces or curves is generally sufficiently complex and dense.

The intruder state problem is further aggravated by the fact that in order to warrant the *size-extensivity* of the method, $\mathcal{M}_0$ should be a *complete model space* (CMS), i.e., should involve *all* possible configurations that result by occupying a chosen set of active orbitals by a given number of valence electrons. Since the dimension of such a CMS rapidly increases with the number of active orbitals (in the same way as does the dimension of the corresponding full configuration interaction (FCI) space), we face not only similarly increasing computational demands, but also heightened likelihood of the occurrence of the intruder states. For this very reason, much attention has been paid to the development of methods that employ truncated or incomplete

model spaces, the extreme case being various *state-selective* CC methods (see, e.g., [3,12]).

The recently formulated MR SU CC approach [13–17] employs a completely *general model space* (GMS) and introduces the concept of the *C-conditions* that represent constraints imposed on the cluster amplitudes associated with the so-called *internal excitations* (i.e., those transforming one reference configuration into another one). These constraints guarantee that the target wave functions become the exact FCI states when no truncation of cluster amplitudes is enforced (see also [9]).

It is well known that the time-independent, second-quantization-based diagrammatic techniques [18] are extremely beneficial not only in the many-body perturbation theory (MBPT), but also in the development of the explicit formalism of the standard SR CC theory (see, e.g., [1,3,5,10–12,19,20]). Indeed, these techniques provide a better insight into the CC formalism and its relationship with the MBPT, are less error prone than the algebraic methods and, most importantly, facilitate the design of efficient codes by readily identifying suitable intermediates. The extension of this technique to the MR formalism, particularly in the GMS SU CC case, is complicated by the absence of a readily identifiable unique Fermi vacuum.

It is the aim of this paper to show how the diagrammatic approach can be modified to yield explicit expressions even in the MR SU CC case, particularly in the least obvious case of the evaluation of the so-called *coupling coefficients*, which involve cluster operators associated with two distinct reference configurations. For this reason, we address these quantities in detail, since other components of the MR SU CC equations can be handled in a similar way as in the SR case.

In section 2, we briefly summarize the essential points of the SU CC method and in section 3 we indicate the modifications characterizing the GMS-based version of this method. We then address the diagrammatic evaluation of the SU CC coupling coefficients, considering first the general expressions in terms of the CI-type components, followed by the explicit expressions in terms of the antisymmetrized cluster amplitudes, considering the most important cases of singly and doubly excited configurations. In this way we re-derive the expressions given in equations (82)–(90) and (93)–(114) of [13] by relying solely on the diagrammatic technique.

2. SU CC method [9]

Using a CMS $\mathcal{M}_0$, $\mathcal{M}_0 = \mathrm{Span}\{|\Phi_i\rangle : i = 1, \ldots, M\}$, the SU cluster Ansatz has the form given by equation (2), in which the cluster operator $T(i)$ that is associated with the reference configuration $|\Phi_i\rangle$ has the standard form in terms

of the excitation operators $G_\ell^{(m)}(i)$,

$$T(i) = \sum_m \sum_\ell t_\ell^{(m)}(i) G_\ell^{(m)}(i)\,, \tag{3}$$

where

$$G_\ell^{(m)}(i)|\Phi_i\rangle = |\Phi_{i;\ell}^{(m)}\rangle \in \mathcal{M}_0^\perp\,. \tag{4}$$

Here, the superscript (m) indicates the excitation level relative to $|\Phi_i\rangle$ and the subscript ℓ enumerates distinct excitation operators and the corresponding configurations $|\Phi_{i;\ell}^{(m)}\rangle$, which belong to the orthogonal complement $\mathcal{M}_0^\perp$ of the CMS $\mathcal{M}_0$. Later on we drop the superscript (m) when it is not essential or when it is obvious from the index set defining the excitation operator. (In any case, the excitation level is not uniquely defined when a spin-adapted formalism is employed. For simplicity's sake we adhere in this paper to the molecular spin orbital (MSO) formalism.)

Within the MSO formalism, the excitation operator $G_\ell^{(m)}(i)$ is fully determined by specifying the MSOs $\{I_1, I_2, \ldots, I_m\}$ that are occupied in $|\Phi_i\rangle$ and are replaced by the MSOs $\{J_1, J_2, \ldots, J_m\}$ that do not constitute $|\Phi_i\rangle$ (assuming a well-defined phase convention), so that ℓ and (m) are implied by the MSO index set

$$\ell \equiv \{J_1, J_2, \ldots, J_m : I_1, I_2, \ldots, I_m\} \tag{5}$$

and

$$G_\ell^{(m)}(i) \equiv G_{I_1 I_2 \ldots I_m}^{J_1 J_2 \ldots J_m}(i) = \prod_{k=1}^{m} (X_{J_k}^\dagger X_{I_k})\,. \tag{6}$$

Thus, in the CMS case, the cluster amplitudes that are associated with the internal excitation operators (i.e., those involving only active MSOs) are set equal to zero by definition, and are thus absent from the expansion of $T(i)$, equation (3), as implied by the requirement given by equation (4).

When we employ the above given SU CC Ansatz for the wave operator U, equations (2)–(4), in the generalized Bloch equation, we obtain the basic equations of the SU CC formalism [9] (see also [1–3]), which can be written in the following compact form

$$\Lambda_m(\ell; i) = \sum_{j(\neq i)} \Gamma^{ij}(\ell; m) H_{ji}^{(\mathrm{eff})}\,, \tag{7}$$

where the left-hand side (LHS) has the form analogous to that characterizing the SR CC equations, i.e.,

$$\Lambda_m(\ell; i) = \langle G_\ell^{(m)}(i)\Phi_i | \bar{H}(i) | \Phi_i \rangle\,, \tag{8}$$

$$\bar{H}(i) = e^{-T(i)} H e^{T(i)} , \tag{9}$$

the $\Gamma^{ij}(\ell; m)$ designates the so-called coupling coefficient

$$\Gamma^{ij}(\ell; m) = \langle G_\ell^{(m)}(i)\Phi_i | e^{-T(i)} e^{T(j)} | \Phi_j \rangle , \tag{10}$$

and $H_{ij}^{(\mathrm{eff})}$ represents the matrix element of the effective Hamiltonian,

$$H_{ij}^{(\mathrm{eff})} = \langle \Phi_i | H e^{T(j)} | \Phi_j \rangle . \tag{11}$$

Once the cluster amplitudes $t_\ell^{(m)}(i) \equiv t_\ell(i)$ are found by solving the SU CC equations (7), one evaluates the effective Hamiltonian $H^{(\mathrm{eff})}$ [including the diagonal elements $H_{ii}^{(\mathrm{eff})} \equiv \Lambda_0(\emptyset; i)$] and determines its eigenvectors $\|C_{ij}\|$, $i = 1, \ldots, M$ and corresponding eigenvalues E_i, $i = 1, \ldots, M$. The target wave functions $|\Psi_i\rangle$, $i = 1, \ldots, M$ are then given by

$$|\Psi_i\rangle = \sum_{j=1}^{M} C_{ij} e^{T(j)} |\Phi_j\rangle . \tag{12}$$

Of course, in actual applications, the expansion for $T(i)$'s is truncated at an appropriate level, usually at the SD (singles and doubles) level, as in the SR CC approach, resulting in the SU CCSD method.

3. GMS SU CC method [13]

When we employ a truncated or *incomplete model space* (IMS) or, in fact, a completely arbitrary model space $\mathcal{M}_0$ which we refer to as a GMS [13–17], we cannot ignore cluster amplitudes that correspond to the excitation operators transforming one reference into another one. We thus distinguish the *internal* and the *external* cluster amplitudes and the corresponding excitation operators, the former ones transforming the configurations spanning $\mathcal{M}_0$ among themselves, while the latter ones are associated with configurations spanning $\mathcal{M}_0^\perp$. We have shown [13–17] that in order to achieve a proper representation of the target states $|\Psi_i\rangle$, $i = 1, \ldots, M$, the internal amplitudes must be determined by the so-called *C-conditions*, representing constraints on the internal cluster amplitudes.

Considering two references $|\Phi_i\rangle$ and $|\Phi_j\rangle$ from $\mathcal{M}_0$ such that

$$|\Phi_i\rangle = G_{P_1 P_2 \ldots P_k}^{Q_1 Q_2 \ldots Q_k} |\Phi_j\rangle , \tag{13}$$

the C-conditions state [13] that the (fully antisymmetrized) internal cluster amplitudes $t_{P_1 P_2 \ldots P_k}^{Q_1 Q_2 \ldots Q_k}(j)$ and $t_{Q_1 Q_2 \ldots Q_k}^{P_1 P_2 \ldots P_k}(i)$ are given by the negative of the products of the corresponding lower-order amplitudes, so that the CI-type coefficient or amplitude $\tau_{P_1 P_2 \ldots P_k}^{Q_1 Q_2 \ldots Q_k}(j)$ [or $\tau_{Q_1 Q_2 \ldots Q_k}^{P_1 P_2 \ldots P_k}(i)$] vanishes, namely

$$\langle \Phi_i | e^{T(j)} | \Phi_j \rangle = \tau_{P_1 P_2 \ldots P_k}^{Q_1 Q_2 \ldots Q_k}(j) \tag{14}$$

$$= t^{Q_1 Q_2 \ldots Q_k}_{P_1 P_2 \ldots P_k}(j) + (\text{a.d.c.}) = 0\,, \tag{15}$$

i.e., that

$$t^{Q_1 Q_2 \ldots Q_k}_{P_1 P_2 \ldots P_k}(j) = -(\text{a.d.c.})\,, \tag{16}$$

and similarly for $t^{P_1 P_2 \ldots P_k}_{Q_1 Q_2 \ldots Q_k}(i)$. Here, the symbol (a.d.c.) stands for *all disconnected clusters* that are associated with the leading cluster amplitude, as implied by the cluster analysis of the FCI wave function [21] (see also [1,3,10,12] and references therein). Thus, all one-body cluster amplitudes $t^{Q_1}_{P_1}(j)$ that are associated with the internal excitations $G^{Q_1}_{P_1}(j)$, (i.e., $|\Phi_i\rangle = G^{Q_1}_{P_1}|\Phi_j\rangle$) must vanish, while for the two-body internal amplitudes $t^{Q_1 Q_2}_{P_1 P_2}(j)$ we have that [13] (dropping the argument j for simplicity)

$$\tau^{Q_1 Q_2}_{P_1 P_2} = t^{Q_1 Q_2}_{P_1 P_2} + t^{Q_1}_{P_1} t^{Q_2}_{P_2} - t^{Q_1}_{P_2} t^{Q_2}_{P_1}\,, \tag{17}$$

implying

$$t^{Q_1 Q_2}_{P_1 P_2} = t^{Q_1}_{P_2} t^{Q_2}_{P_1} - t^{Q_1}_{P_1} t^{Q_2}_{P_2}\,, \tag{18}$$

where we assumed that $|\Phi_i\rangle = G^{Q_1 Q_2}_{P_1 P_2}|\Phi_j\rangle$, $|\Phi_i\rangle, |\Phi_j\rangle \in \mathcal{M}_0$. In general, we have that

$$(\text{a.d.c.}) \equiv \sum_{\mathfrak{P}_k} \prod_{\ell=1}^{p} \langle \Phi_i | (n_\ell!)^{-1} [T_\ell(j)]^{n_\ell} | \Phi_j \rangle\,, \tag{19}$$

where the sum extends over all nontrivial partitions $\mathfrak{P}_k$ of k, and $k = \sum_{\ell=1}^{p} \ell \cdot n_\ell$ with $0 \leqslant n_\ell \leqslant k$, $1 \leqslant p < k$.

Thus, in the GMS SU CC approach, only the external cluster amplitudes are determined via the SU CC equations (7), while the internal amplitudes are given by the C-conditions.

4. Explicit form of the GMS SU CCSD equations

We are now ready to consider the explicit form of the GMS SU CC equations. We first briefly address the LHS of equation (7) and the effective Hamiltonian matrix elements, and subsequently focus on the evaluation of the coupling coefficients, equation (10).

4.1. Evaluation of $\Lambda_m(\ell; i)$ and $H_{ij}^{(\mathrm{eff})}$

The LHS of the SU CC equations, equation (7), is given by the expression for $\Lambda_m(\ell; i)$, equations (8) and (9), which in the specific case of ℓ and m given by equation (5) can be rewritten as follows

$$\Lambda(I_1, I_2, \ldots, I_m : J_1, J_2, \ldots, J_m; i) = \langle G^{J_1 J_2 \ldots J_m}_{I_1 I_2 \ldots I_m}(i)\Phi_i | e^{-T(i)} H e^{T(i)} | \Phi_i \rangle \,. \quad (20)$$

This expression has the same form as the LHS of SR CC equations, the only difference being that we now deal with different references $|\Phi_i\rangle$. However, considering each reference as a new Fermi vacuum, this LHS will have the same form as in the SR case when expressed in terms of the $t(i)$ cluster amplitudes. In fact, we can even use the actual SR CC codes after making suitable changes.

Similarly, the diagonal elements of the effective Hamiltonian (which are only needed in the last step; see above) are also given by the same expressions as in the SR case. In fact, we have that

$$H_{ii}^{(\mathrm{eff})} = \Lambda_0(\emptyset; i) = \langle \Phi_i | \overline{H} | \Phi_i \rangle = \langle \Phi_i | H e^{T(i)} | \Phi_i \rangle \quad (21)$$

$$= \langle \Phi_i | H (1 + T(i) + \tfrac{1}{2}[T(i)]^2) | \Phi_i \rangle \,. \quad (22)$$

Moreover, the expressions for Λ_k can be exploited in the evaluation of the off-diagonal elements of $H^{(\mathrm{eff})}$, as shown in [13], where the diagrammatic version was also presented. For example, when $|\Phi_i\rangle$ and $|\Phi_j\rangle$ differ in two MSO, so that $|\Phi_i\rangle = G^{Q_1 Q_2}_{P_1 P_2} |\Phi_j\rangle$, it can be shown [13] that

$$H_{ij}^{(\mathrm{eff})} = \langle \Phi_i | H e^{T(j)} | \Phi_j \rangle \quad (23)$$

$$= \Lambda_2(P_1 P_2 : Q_1 Q_2; j) + \mathbf{P}_{Q_1 Q_2} \mathbf{P}_{P_1 P_2} t^{Q_1}_{P_1}(j)\, \Lambda_1(P_2 : Q_2; j) \,, \quad (24)$$

where

$$\mathbf{P}_{XY} = 1 - (XY) \,, \quad (25)$$

with (XY) representing the transposition of X and Y. The diagrammatic representation also implies (cf. figures 1 and 2 of [13]) that the disconnected component [which is given by the expression $\tau^{Q_1 Q_2}_{P_1 P_2}(j) H^{(\mathrm{eff})}_{jj}$ in the above presented example, equation (24)] vanishes thanks to the relevant C-condition.

We can thus turn our attention to the evaluation of the coupling coefficients, equation (10).

4.2. Evaluation of coupling coefficients

Consider a general coupling coefficient $\Gamma^{ij}(\ell; m)$, equation (10), which in the case that $G^{(m)}_{\ell}(i)$ is given by equation (6) we write in a more explicit form,

namely

$$\Gamma^{ij}(\ell; m) \equiv \Gamma_k(J_1 J_2 \ldots J_m : I_1 I_2 \ldots I_m) \tag{26}$$

$$= \langle G^{J_1 J_2 \ldots J_m}_{I_1 I_2 \ldots I_m}(i)\Phi_i | e^{-T(i)} e^{T(j)} | \Phi_j \rangle \,, \tag{27}$$

where we now drop the superscripts i and j since they are apparent from the context and introduce the subscript k indicating that the configurations $|\Phi_i\rangle$ and $|\Phi_j\rangle$ differ in k MSOs, so that we can write

$$|\Phi_i\rangle = |\{(AB\ldots)Q_1 Q_2 \ldots Q_k\}\rangle \,, \tag{28}$$

$$|\Phi_j\rangle = |\{(AB\ldots)P_1 P_2 \ldots P_k\}\rangle \,. \tag{29}$$

Here, the braces imply the antisymmetrization of the spin-orbital product and the symbol $(AB\ldots)$ designates the MSOs that are common to both references related via equation (13) or, equivalently, via

$$|\Phi_j\rangle = G^{P_1 P_2 \ldots P_k}_{Q_1 Q_2 \ldots Q_k} |\Phi_i\rangle \,. \tag{30}$$

As explained in [13], we refer to the MSOs $|A\rangle, |B\rangle, |C\rangle$, etc. that are occupied in both references (28) and (29) as the *local core* spin orbitals, while those occupied either in $|\Phi_i\rangle$ or in $|\Phi_j\rangle$, but not in both (i.e., those labelled by P_μ's and Q_μ's in our case), represent the *local active* MSOs. Those MSOs which are not occupied in either configuration (28) or (29) then represent the *local virtual* MSOs and are labelled by R, S, T, etc. Thus, the MSOs $|I_\mu\rangle$ that are labelled by I_μ, $\mu = 1, \ldots, m$, in equation (27), can be either local core MSOs (i.e., $|A\rangle, |B\rangle, |C\rangle \ldots$) or local active MSOs $|Q_\mu\rangle$, $\mu = 1, \ldots, k$. Similarly, those labelled by J_μ, $\mu = 1, \ldots, m$, can represent either local virtual MSOs (i.e., $|R\rangle, |S\rangle, |T\rangle, \ldots$) or local active MSOs $|P_\mu\rangle$, $\mu = 1, \ldots, k$. The same rules apply, of course, to the excitation operators that define the cluster operator $T(i)$.

Using equation (30), we can rewrite the expression for the coupling coefficient $\Gamma^{ij}(\ell; m)$, equation (27), as a mean value in the state $|\Phi_i\rangle$, namely

$$\Gamma_k(J_1 J_2 \ldots J_m : I_1 I_2 \ldots I_m) = \langle G^{J_1 J_2 \ldots J_m}_{I_1 I_2 \ldots I_m}(i)\Phi_i | e^{-T(i)} e^{T(j)} G^{P_1 P_2 \ldots P_k}_{Q_1 Q_2 \ldots Q_k} | \Phi_i \rangle$$

$$= \langle \Phi_i | G^{I_1 I_2 \ldots I_m}_{J_1 J_2 \ldots J_m}(i) e^{-T(i)} e^{T(j)} G^{P_1 P_2 \ldots P_k}_{Q_1 Q_2 \ldots Q_k} | \Phi_i \rangle \,. \tag{31}$$

Following standard diagrammatic rules (see, e.g., [1,3,10–12,18–20,22,23] and references therein) we now represent the bra-state $\langle G^{J_1 J_2 \ldots J_m}_{I_1 I_2 \ldots I_m}(i)\Phi(i)|$ by the diagram (a) of figure 1 and, similarly, the ket-state $|\Phi_j\rangle = G^{P_1 P_2 \ldots P_k}_{Q_1 Q_2 \ldots Q_k} |\Phi_i\rangle$ by the diagram (b) of the same figure.

Recall that the creation operators [cf. equation (6)] are associated with the oriented lines leaving a given vertex, while those corresponding to annihilation operators enter the vertex. Moreover, the hole lines (core or active relative to

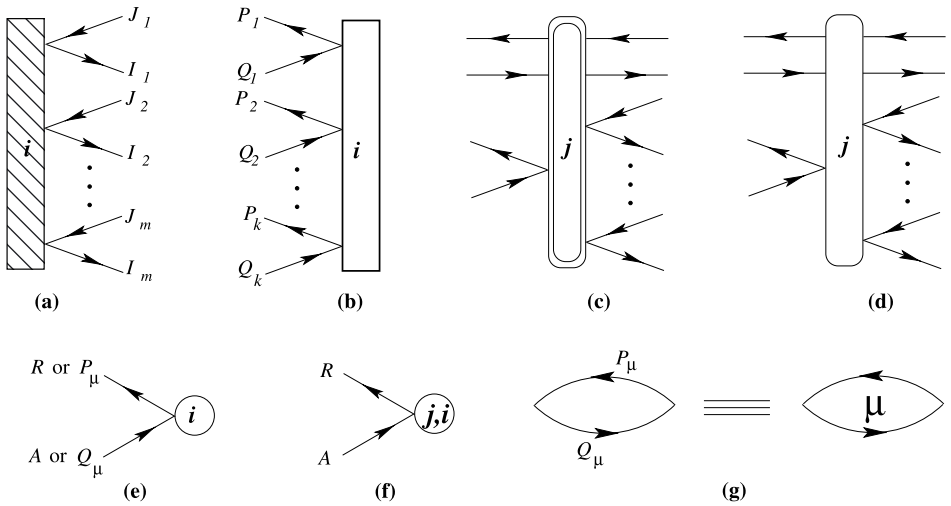

Figure 1. A schematic representation of various vertices used in the evaluation of the SU CC coupling coefficients. See the text for details.

$|\Phi_i\rangle$ as a Fermi vacuum) are directed from the left to the right, while the particle lines are heading in the opposite direction. We shall refer to the vertices (a) and (b) of figure 1 as the bra and ket vertices, respectively. (Strictly speaking, all the vertices that we employ are in fact super-vertices consisting of a number of simple vertices, each involving one entering and one leaving the fermion line [10,11,18,20,22,23].)

In a similar way, we associate with the fully antisymmeterized CI-type τ-coefficients or amplitudes, equations (14) and (15), the oval-shaped i or j τ-vertices of a general kind shown in figure 1(c) and, similarly, the CC-type t-amplitudes we represent via the t-vertices shown in figure 1(d). Note that in each case we employ Goldstone-type vertices, since they can be easily converted to those of the Hugenholtz type by shrinking them to a single point-like vertex. In actual evaluations of the considered quantities we employ the so-called Brandow approach, in which we represent each Hugenholtz diagram by one of its "antisymmetrized" Goldstone versions (irrespective of which one). In this way we can benefit from a small number of Hugenholtz diagrams (i.e., from the fully antisymmetrized formalism) and yet properly determine the correct phase of each term.

To evaluate the desired quantities, we thus have to construct all resulting, topologically inequivalent, connected diagrams and associate with them the algebraic expressions following the standard rules. Since all the lines in our diagrams carry the fixed labels, so that no free labels are present, there are no summations over the free labels and all the weights are equal to 1. The phase is given by the

usual factor $(-1)^{\ell+h}$, where ℓ is the number of closed loops of oriented lines and h designates the number of hole lines. (Note that in the present case all fermion lines are of the internal kind.) An extra factor of (-1) is then associated with each i-type t-vertex, arising from the fact that $e^{-T(i)} = 1 - T(i) + \frac{1}{2}[T(i)]^2 - \frac{1}{3!}[T(i)]^3 + \ldots$. We shall see, however, that in all diagrams considered here at most one τ or t vertex of this kind can appear.

In constructing the resulting diagrams, we have to respect the following rules for the labelling of oriented lines (cf. equation (31)):

(i) *Bra-vertex* [figure 1(a)]: All fermion lines extend to the RHS of this vertex and carry either the core or virtual labels. In addition, the outgoing lines can also carry the active labels Q_μ and the ingoing ones the active labels P_μ. Note, however, that in the case that only active labels P_μ and Q_μ, $\mu = 1, \ldots, \kappa$ are present, implying the excitation order κ for the bra-state, we must have that $k > \kappa$, and similar restrictions apply even when only some P_μ and/or Q_μ labels are present in addition to the core and virtual ones (see below). No algebraic expression is associated with this vertex when evaluating the resulting diagrams.

(ii) *Ket vertex* [figure 1(b)]: Only P_μ and Q_μ, $\mu = 1, \ldots, k$ labels are present, Q_μ's labelling the ingoing lines and P_μ's the outgoing ones. Again, no algebraic expression is associated with this vertex when evaluating the resulting diagrams.

(iii) $\tau(j)$ *or* $t(j)$ *vertices* [figure 1(c) or 1(d), respectively]: The lines attached to the LHS (issuing from the bra-vertex) can carry only core or virtual MSO labels; those attached to the RHS are invariably the active MSO labels (P_μ's for ingoing and Q_μ's for outgoing lines). The algebraic expressions associated with these vertices are the $\tau(j)$ or $t(j)$ amplitudes whose superscripts (subscripts) are given by the MSO labels on the outgoing (ingoing) fermion lines. Each pair of corresponding superscripts and subscripts is associated with a pair of oriented lines that enter and leave the same point (or vertex) of a given $\tau(j)$ or $t(j)$ (super)vertex. The $\tau(j)$ and $t(j)$ amplitudes are antisymmetric with respect to any separate permutation of their subscripts and superscripts and thus invariant to simultaneous permutations of *corresponding pairs* of super- and sub-scripts.

(iv) $\tau(i)$ *or* $t(i)$ *vertices* [figure 1(e) or 1(f)]: All the fermion lines extend to the LHS of these vertices and can carry any MSO label. However, P_μ's must label the outgoing and Q_μ's the ingoing lines. In all cases considered in this work, only the vertices representing the type shown in figure 1(e) [or 1(f) for combined $t(i)$ and $t(j)$ vertices, see below] can arise. The algebraic expression that is associated with these vertices is given by the same rule as in the preceding case (iii).

Note that in all cases just mentioned the core, active or virtual MSOs stand for *local* core, *local* active or *local* virtual MSOs, respectively. To simplify the resulting diagrams, we employ a simplified labelling of closed loops that involve only the corresponding particle and hole lines issuing from the same vertex of the ket-supervertex i and carry the labels P_μ and Q_μ, $\mu = 1, 2, \ldots, k$, respectively, as shown in the diagram (g) of figure 1.

In the following, we first consider general expressions for $\Gamma_k(\ell)$ with an arbitrary k in terms of the CI-type $\tau(j)$ and $\tau(i)$ vertices or amplitudes and, subsequently, we derive the explicit expressions in terms of the antisymmetrized $t(j)$ and $t(i)$ vertices or amplitudes. In all cases, we only consider at most a doubly excited submanifold of $\mathcal{M}_0^\perp$. This provides us with all necessary expressions for the SU CCSD method, assuming that the reference configurations also differ in at most two MSOs (i.e., for $k = 2$). These results provide sufficient illustration of the diagrammatic approach to the SU CC formalism and can be easily extended to a higher excitation order if required. They also provide ample illustration of the role of the C-conditions for the disappearance of disconnected terms.

4.2.1. General expressions

We first consider a general case involving model-space references $|\Phi_i\rangle$ and $|\Phi_j\rangle$ differing in k MSOs, equations (28)–(31), while restricting the excited state submanifold $\mathcal{M}_0^\perp$ to at most doubles, i.e., $m = 1$ and 2. In each case, we have to distinguish four types of excitations, namely the core to active, core to virtual, active to virtual, and the active to active ones (all in the "local" sense relative to the configurations $|\Phi_i\rangle$ and $\Phi_j\rangle$ involved).

(i) *Single excitations*

To obtain the expressions for the coupling coefficients given by equations (78)–(81) of [13], we construct the resulting diagrams shown in figure 2 and evaluate them as indicated in table 1. Note that only connected diagrams are shown, since contributions from the disconnected diagrams invariably vanish in view of the C-conditions. For example, in the case of $\Gamma_k(P_1 : A)$, we obtain in addition to the diagram (a) of figure 2 also the disconnected diagram shown in figure 3(a). Similar disconnected diagrams arise for $\Gamma_k(R{:}Q_1)$ and $\Gamma_k(R : A)$, always containing a subdiagram (b) of figure 3, which contributes the $\tau(j)$ vanishing amplitude, equation (15). Finally, note that the coupling coefficient $\Gamma_k(P_1 : Q_1)$ can only arise when $k > 1$.

(ii) *Double excitations*

Considering, next, the double excitations, we have to distinguish different cases depending on the magnitude of k, equations (28)–(31). For an arbitrary $k \geqslant 1$, we have four distinct cases represented by equations (82)–(85) of [13]. To reduce the number of resulting diagrams that only differ by the labelling of nonequivalent lines, we exploit the permutation operators $\mathbf{P}_{XY}$ defined by equation (25). Note that these operators are most easily determined from the Hugenholtz version of each diagram, since they pertain to the MSO labels that

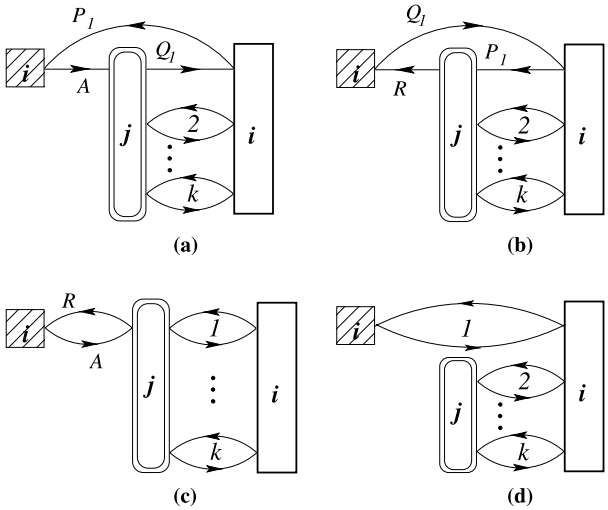

Figure 2. Resulting diagrams for the coupling coefficients $\Gamma_k(J_1 \ : \ I_1)$ for the core-active (a), active-virtual (b), core-virtual (c), and active-active (d) excitations. The corresponding algebraic expressions in terms of the τ-amplitudes are given in table 1.

Table 1
Algebraic expressions for $\Gamma_k(J_1 : I_1)$ associated with diagrams of figure 2.

Coupling coefficient	Diagram (figure 2)	Contribution
$\Gamma_k(P_1 : A)$	(a)	$-\tau^{Q_1 Q_2 \ldots Q_k}_{A P_2 \ldots P_k}(j)$
$\Gamma_k(R : Q_1)$	(b)	$\tau^{R Q_2 \ldots Q_k}_{P_1 P_2 \ldots P_k}(j)$
$\Gamma_k(R : A)$	(c)	$\tau^{R Q_1 \ldots Q_k}_{A P_1 \ldots P_k}(j)$
$\Gamma_k(P_1 : Q_1),\ k > 1$	(d)	$\tau^{Q_2 \ldots Q_k}_{P_2 \ldots P_k}(j)$

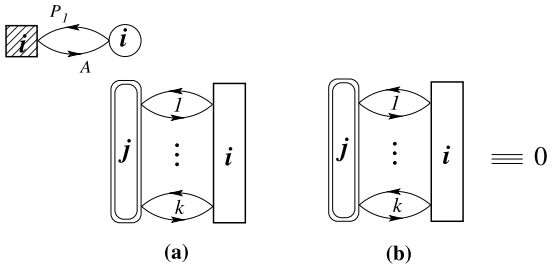

Figure 3. An example of disconnected contributions (a). Such contributions vanish in view of the C-conditions, equation (15), represented diagrammatically in (b).

Table 2
Algebraic expressions for $\Gamma_k(J_1 J_2 : I_1 I_2)$ associated with diagrams of figure 4.

Coupling coefficient	Diagram (figure 4)	Contribution
$\Gamma_k(P_1 R : AB)$	(a_1)	$-\tau^{Q_1 R Q_2 \ldots Q_k}_{A B P_2 \ldots P_k}(j) = \tau^{R Q_1 Q_2 \ldots Q_k}_{A B P_2 \ldots P_k}(j)$
	(a_2)	$\mathbf{P}_{AB} t^R_B(i)\, \tau^{Q_1 Q_2 \ldots Q_k}_{A P_2 \ldots P_k}(j)$
		$= -\mathbf{P}_{AB} t^R_A(i)\, \tau^{Q_1 Q_2 \ldots Q_k}_{B P_2 \ldots P_k}(j)$
	(a_3)	$-\mathbf{P}_{AB} t^{P_1}_A(i)\, \tau^{R Q_1 \ldots Q_k}_{B P_1 \ldots P_k}(j)$
$\Gamma_k(RS : AQ_1)$	(b_1)	$\tau^{R S Q_2 \ldots Q_k}_{A P_1 P_2 \ldots P_k}(j)$
	(b_2)	$-\mathbf{P}_{RS} t^R_A(i)\, \tau^{S Q_2 \ldots Q_k}_{P_1 P_2 \ldots P_k}(j)$
	(b_3)	$-\mathbf{P}_{RS} t^S_{Q_1}(i)\, \tau^{R Q_1 \ldots Q_k}_{A P_1 \ldots P_k}(j)$
		$= \mathbf{P}_{RS} t^R_{Q_1}(i)\, \tau^{S Q_1 \ldots Q_k}_{A P_1 \ldots P_k}(j)$
$\Gamma_k(RP_1 : AQ_1)$	(c_1)	$\tau^{R Q_2 \ldots Q_k}_{A P_2 \ldots P_k}(j)$
	(c_2)	$-t^R_A(i)\, \tau^{Q_2 \ldots Q_k}_{P_2 \ldots P_k}(j)$
	(c_3)	$-t^{P_1}_{Q_1}(i)\, \tau^{R Q_1 \ldots Q_k}_{A P_1 \ldots P_k}(j)$
	(c_4)	$t^{P_1}_A(i)\, \tau^{R Q_2 \ldots Q_k}_{P_1 P_2 \ldots P_k}(j)$
	(c_5)	$-t^R_{Q_1}(i)\, \tau^{Q_1 Q_2 \ldots Q_k}_{A P_2 \ldots P_k}(j)$
$\Gamma_k(RS : AB)$	(d_1)	$\tau^{R S Q_1 \ldots Q_k}_{A B P_1 \ldots P_k}(j)$
	(d_2)	$-\mathbf{P}_{RS} \mathbf{P}_{AB} t^R_A(i)\, \tau^{S Q_1 \ldots Q_k}_{B P_1 \ldots P_k}(j)$

are associated with nonequivalent fermion lines of the corresponding nonlabelled diagram (also called a skeleton [10]).

The relevant resulting diagrams are shown in figures 4 and 5, and their algebraic equivalents are listed in tables 2 and 3, respectively. Again, a number of disconnected diagrams can arise (e.g., for diagrams analogous to (a_3), (b_3), (c_5), and (d_2) of figure 4, all involving a subdiagram (b) of figure 3 and thus yielding a vanishing contribution in view of the pertinent C-condition). It should also be noted that in the Hugenholtz version of diagram (a_1) of figure 4, the hole lines labelled by A and B represent equivalent lines, but not in diagrams (a_2) and (a_3) of the same figure, thus yielding two nonequivalent versions which are encompassed via the operator $\mathbf{P}_{AB}$, equation (25), and similarly for other

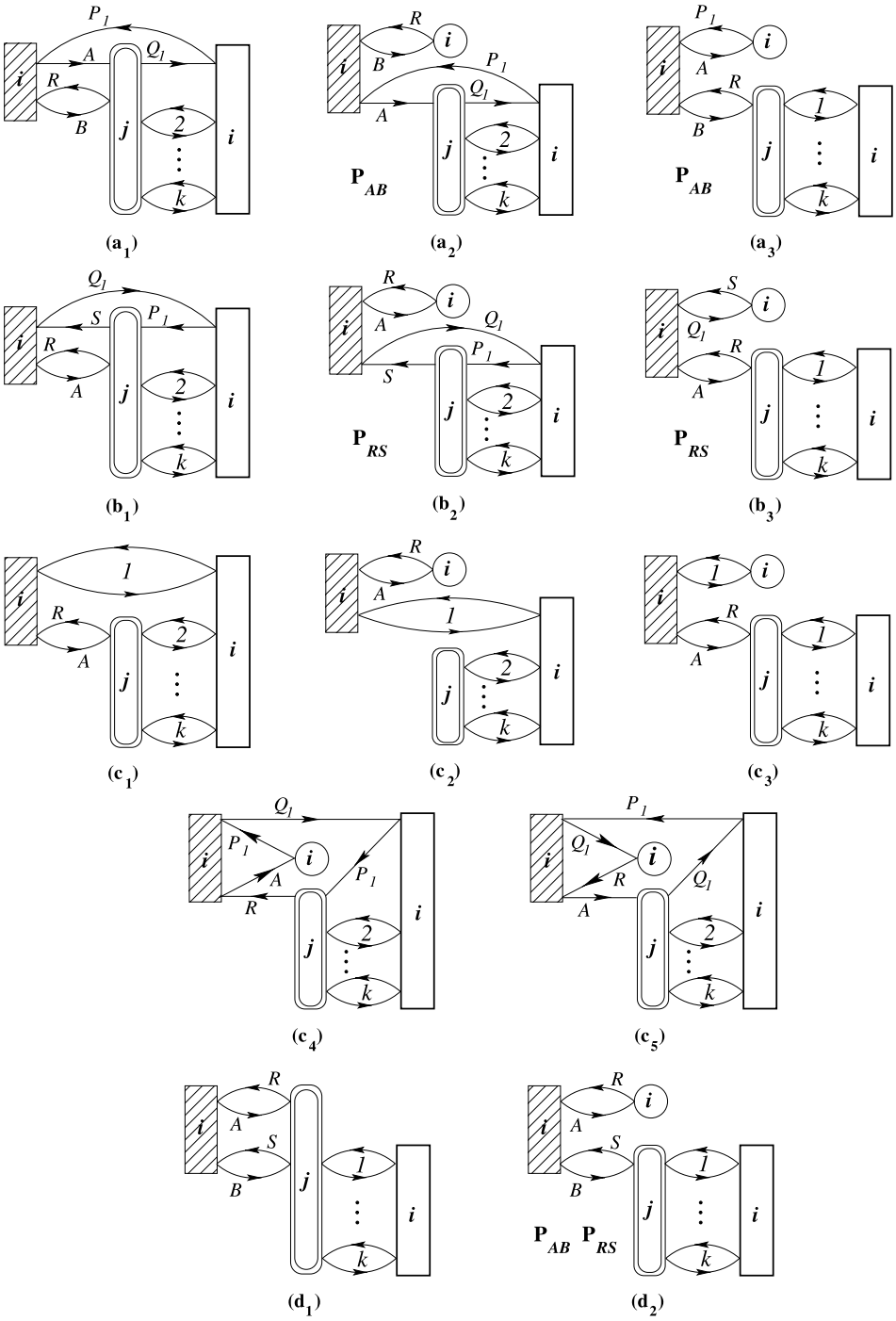

Figure 4. Resulting diagrams for the coupling coefficients $\Gamma_k(J_1J_2 : I_1I_2)$, $k \geqslant 1$, corresponding to equations (82)–(85) of [13]. The associated algebraic expressions are given in table 2.

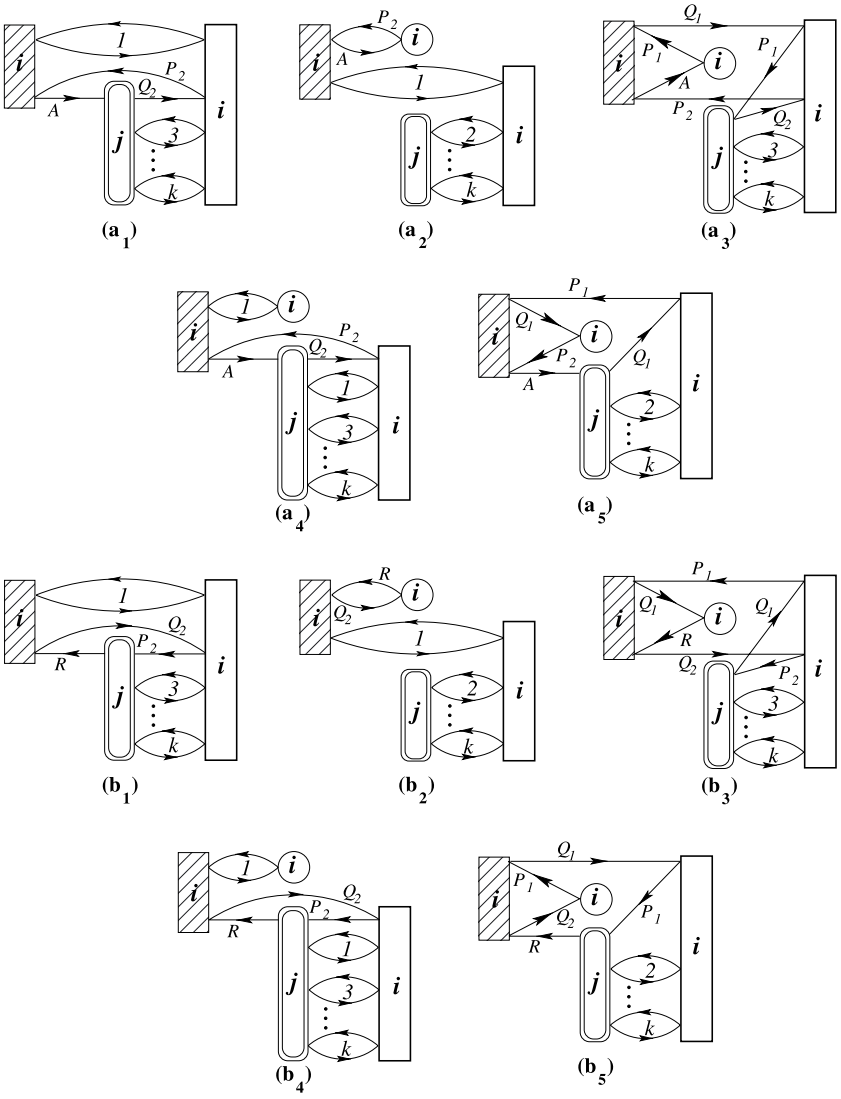

Figure 5. Resulting diagrams for the coupling coefficients $\Gamma_k(J_1J_2 : I_1I_2), k \geqslant 2$, corresponding to equations (86)–(90) of [13]. The associated algebraic expressions are given in table 3. In diagrams (e_2) and (e_3) we define $\overline{\mu} = 3 - \mu$ with $\mu = 1, 2$.

diagrams. The first four coupling coefficients listed in table 3 and figure 5 can only arise when $k > 1$ and the last one only when $k > 2$. In those cases no disconnected diagrams arise.

Finally, we note a sign misprint in two of the expressions given in [13], namely the second term on the RHS of equation (83) should have a plus sign, as well as the last term on the RHS of equation (87) [the corresponding terms are (b_3) in table 2 and (b_4), (b_5) in table 3].

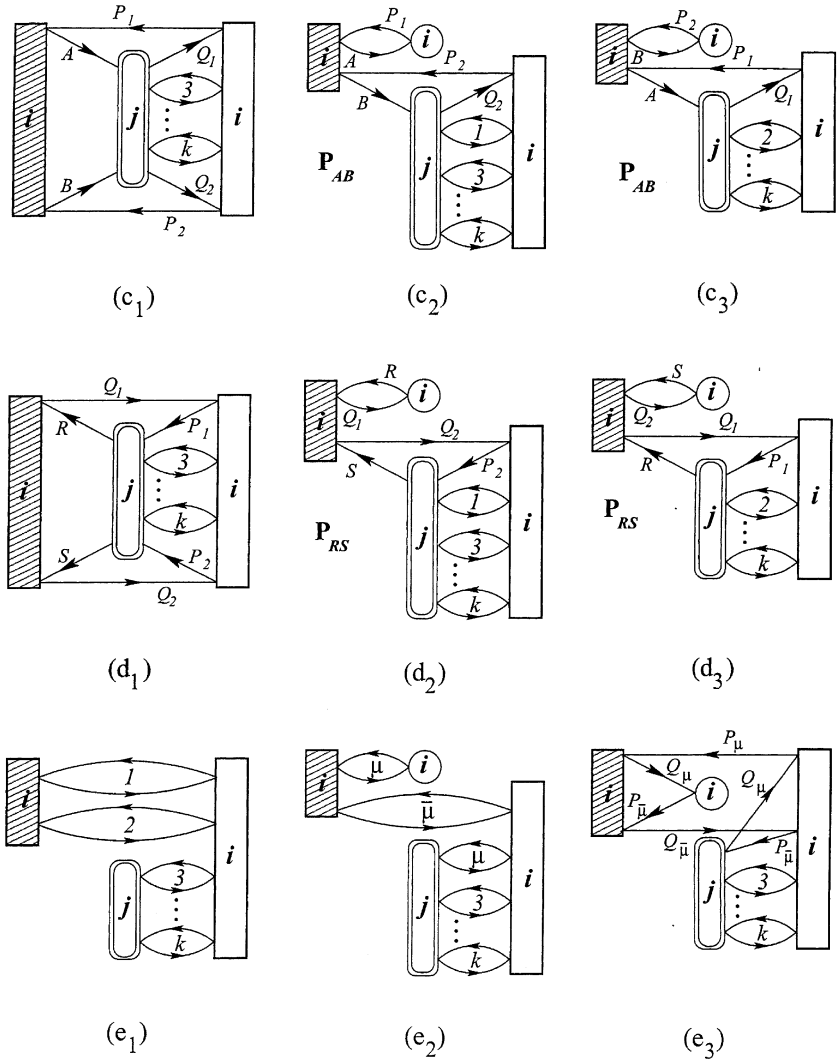

Figure 5. *continued*

4.2.2. Explicit expressions

Although the above given expressions in terms of $\tau(j)$ coefficients are very compact, in actual implementations we often require the explicit expressions in terms of the $t(i)$ and $t(j)$ amplitudes. Indeed, in the CCSD case, we truncate the cluster amplitudes at the two-body level. Moreover, for sufficiently large k values, the $\tau(j)$ coefficients involve a number of disconnected terms and the general expressions, equations (82)–(90) of [13], contain a number of vanishing terms that are associated with disconnected resulting diagrams.

Table 3
Algebraic expressions for $\Gamma_k(J_1 J_2 : I_1 I_2)$ associated with diagrams of figure 5. We define $\overline{\mu} = 3 - \mu$, $\mu = 1, 2$.

Coupling coefficient	Diagram (figure 5)	Contribution
$\Gamma_k(P_1P_2:Q_1A), k>1$	(a_1)	$-\tau_{A\,P_3\ldots P_k}^{Q_2Q_3\ldots Q_k}$
	(a_2) (a_3)	$\left.\begin{array}{l} -t_A^{P_2}(i)\,\tau_{P_2\ldots P_k}^{Q_2\ldots Q_k}(j) \\ -t_A^{P_1}(i)\,\tau_{P_1P_3\ldots P_k}^{Q_2Q_3\ldots Q_k}(j) \end{array}\right\} - \sum_{\mu=1}^{2} t_A^{P_\mu}(i)\,\tau_{P_\mu P_3\ldots P_k}^{Q_2Q_3\ldots Q_k}(j)$
	(a_4) (a_5)	$\left.\begin{array}{l} t_{Q_1}^{P_1}(i)\,\tau_{A\,P_1P_3\ldots P_k}^{Q_2Q_1Q_3\ldots Q_k}(j) \\ -t_{Q_1}^{P_2}(i)\,\tau_{A\,P_2P_3\ldots P_k}^{Q_1Q_2Q_3\ldots Q_k}(j) \end{array}\right\} - \sum_{\mu=1}^{2} t_{Q_1}^{P_\mu}(i)\,\tau_{A\,P_\mu P_3\ldots P_k}^{Q_1Q_2Q_3\ldots Q_k}(j)$
$\Gamma_k(P_1R:Q_1Q_2), k>1$	(b_1)	$\tau_{P_2P_3\ldots P_k}^{R\,Q_3\ldots Q_k}(j)$
	(b_2) (b_3)	$\left.\begin{array}{l} -t_{Q_2}^{R}(i)\,\tau_{P_2P_3\ldots P_k}^{Q_2Q_3\ldots Q_k}(j) \\ -t_{Q_1}^{R}(i)\,\tau_{P_2P_3\ldots P_k}^{Q_1Q_3\ldots Q_k}(j) \end{array}\right\} - \sum_{\mu=1}^{2} t_{Q_\mu}^{R}(i)\,\tau_{P_2P_3\ldots P_k}^{Q_\mu Q_3\ldots Q_k}(j)$
	(b_4) (b_5)	$\left.\begin{array}{l} -t_{Q_1}^{P_1}(i)\,\tau_{P_2P_1P_3\ldots P_k}^{R\,Q_1Q_3\ldots Q_k}(j) \\ t_{Q_2}^{P_1}(i)\,\tau_{P_1P_2\ldots P_k}^{R\,Q_2\ldots Q_k}(j) \end{array}\right\} \sum_{\mu=1}^{2} t_{Q_\mu}^{P_1}(i)\,\tau_{P_1P_2P_3\ldots P_k}^{R\,Q_\mu Q_3\ldots Q_k}(j)$
$\Gamma_k(P_1P_2:AB), k>1$	(c_1)	$\tau_{A\,B\,P_3\ldots P_k}^{Q_1Q_2Q_3\ldots Q_k}(j)$
	(c_2) (c_3)	$\left.\begin{array}{l} \mathbf{P}_{AB}t_A^{P_1}(i)\,\tau_{B\,P_1P_3\ldots P_k}^{Q_2Q_1Q_3\ldots Q_k}(j) \\ \mathbf{P}_{AB}t_B^{P_2}(i)\,\tau_{A\,P_2\ldots P_k}^{Q_1Q_2\ldots Q_k}(j) \end{array}\right\} - \mathbf{P}_{AB}\sum_{\mu=1}^{2} t_A^{P_\mu}(i)\,\tau_{B\,P_\mu P_3\ldots P_k}^{Q_1Q_2Q_3\ldots Q_k}(j)$
$\Gamma_k(RS:Q_1Q_2), k>1$	(d_1)	$\tau_{P_1P_2P_3\ldots P_k}^{R\,S\,Q_3\ldots Q_k}(j)$
	(d_2) (d_3)	$\left.\begin{array}{l} -\mathbf{P}_{RS}t_{Q_1}^{R}(i)\,\tau_{P_2P_1P_3\ldots P_k}^{S\,Q_1Q_3\ldots Q_k}(j) \\ -\mathbf{P}_{RS}t_{Q_2}^{S}(i)\,\tau_{P_1P_2\ldots P_k}^{R\,Q_2\ldots Q_k}(j) \end{array}\right\} \mathbf{P}_{RS}\sum_{\mu=1}^{2} t_{Q_\mu}^{R}(i)\,\tau_{P_1P_2P_3\ldots P_k}^{S\,Q_\mu Q_3\ldots Q_k}(j)$
$\Gamma_k(P_1P_2:Q_1Q_2), k>2$	(e_1)	$\tau_{P_3\ldots P_k}^{Q_3\ldots Q_k}(j)$
	(e_2) (e_3)	$\left.\begin{array}{l} -\sum_{\mu=1}^{2} t_{Q_\mu}^{P_\mu}(i)\,\tau_{P_\mu P_3\ldots P_k}^{Q_\mu Q_3\ldots Q_k}(j) \\ -\sum_{\mu=1}^{2} t_{Q_\mu}^{P_{\overline{\mu}}}(i)\,\tau_{P_{\overline{\mu}}P_3\ldots P_k}^{Q_\mu Q_3\ldots Q_k}(j) \end{array}\right\} - \sum_{\mu,\nu=1}^{2} t_{Q_\mu}^{P_\nu}(i)\,\tau_{P_\nu P_3\ldots P_k}^{Q_\mu Q_3\ldots Q_k}(j)$

To derive the explicit expressions for the coupling coefficients, we now restrict our considerations to references that differ in at most two MSOs, i.e., to the cases $k = 1$ and $k = 2$. Thus, in addition to distinguishing different types of local excitations (core-active, etc., of both pure and mixed types) as in the general case, we also have to distinguish cases of different k values, namely the cases corresponding to $k = 1$ and $k = 2$. For greater compactness, we also introduce the quantity $w_A^R(ji)$,

$$w_A^R(ji) = t_A^R(j) - t_A^R(i)\,, \tag{32}$$

which we represent by the diagram (f) of figure 1.

The construction of the resulting diagrams in terms of the $t(i)$ and $t(j)$ vertices and their subsequent evaluation in terms of the corresponding cluster amplitudes, yielding the explicit expressions for the coupling coefficients, may be achieved in essentially two ways: We can either exploit the general diagrams and formulas that have been derived in the preceding subsection or we can construct the relevant diagrams from the outset, starting with the bra- and ket-vertices in addition to one or more t-vertices. This latter procedure is best carried out in stages by first drawing the nonoriented diagrams of the Hugenholtz type, which can be easily classified by the number of t-vertices employed and by the possible graph theoretical connection schemes and, in the second step, by introducing all possible orientations of fermion lines, while choosing one Goldstone representative for each Hugenholtz diagram. Such a procedure is particularly useful in more complex cases when a considerable number of diagrams must be accounted for, as will be illustrated below on a suitable example.

Proceeding in either of these ways, we can make certain that no resulting diagram has been missed. The mutual cancellation of disconnected terms occurs automatically and can be checked in an algebraic way. We can thus proceed to consider the relevant cases and re-derive the expressions given by equtions (93)–(94) and (103)–(114) of [13] using the diagrammatic technique. We shall present directly the required resulting diagrams and the corresponding algebraic expressions they represent, and only in the most laborious case of the coupling coefficient $\Gamma_2(RS\ :\ AB)$, equation (114) of [13], we shall illustrate the above mentioned multistage process of diagram construction. Should the reader be unable to construct the resulting diagrams in other cases directly, he can – for pedagogical reasons – always proceed in the reverse direction and convert the final resulting diagrams given below into the Hugenholtz-type nonoriented ones and, after eliminating the equivalent ones, to start from the very beginning with the bra and ket vertices and the $t(i)$ and $t(j)$ vertices of different valency.

(i) $k = 1$ *case*

Writing

$$|\Phi_i\rangle = |\{(AB\ldots)Q\}\rangle\,, \tag{33}$$

and

$$|\Phi_j\rangle = |\{(AB\ldots)P\}\rangle\,, \tag{34}$$

we choose appropriate bra and ket vertices and systematically generate the nonoriented Hugenholtz diagrams for singly and doubly excited bra-configurations of various (i.e., core-active, core-virtual, etc., as well as mixed) types. Orienting

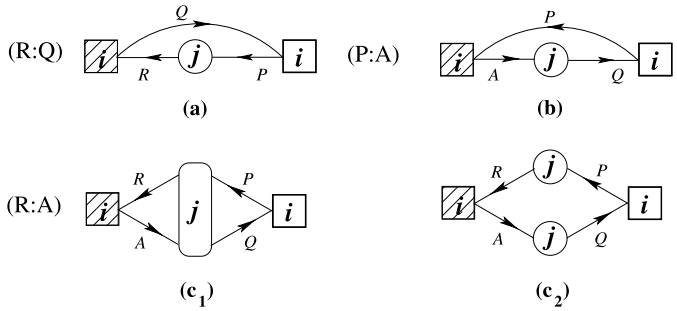

Figure 6. Resulting diagrams for the coupling coefficients $\Gamma_1(J:I)$, corresponding to equations (93)–(95) of [13]. Their algebraic equivalents are listed in table 4.

Table 4
Algebraic expressions for $\Gamma_1(J{:}I)$ associated with diagrams of figure 6.

Coupling coefficient	Diagram (figure 6)	Contribution
$\Gamma_1(R:Q)$	(a)	$t_P^R(j)$
$\Gamma_1(P:A)$	(b)	$-t_A^Q(j)$
$\Gamma_1(R:A)$	(c_1)	$-t_{PA}^{RQ}(j)$
	(c_2)	$-t_P^R(j)\,t_A^Q(j)$

the fermion lines in all possible ways we then easily generate a Goldstone representation of each Hugenholtz diagram. For the monoexcited case, these diagrams are shown in figure 6 and for the doubly excited case in figure 7, while the results of their evaluation are listed in tables 4 and 5, respectively. It is then easy to verify that these results recover the algebraically generated expressions given by equations (93)–(99) of [13].

(ii) $k = 2$ *case*

In this case, equtions (28) and (29) become

$$|\Phi_i\rangle = |\{(AB\ldots)Q_1Q_2\}\rangle\,, \tag{35}$$

and

$$|\Phi_j\rangle = |\{(AB\ldots)P_1P_2\}\rangle\,. \tag{36}$$

For the sake of brevity we present in the following only the resulting diagrams of the Brandow-type (one Goldstone representative for each Hugenholtz diagram) and only in the most laborious case of the $\Gamma_2(RS:AB)$ coefficient we also show their systematic generation starting with nonoriented Hugenholtz diagrams.

For the singly-excited bra-configurations, the resulting diagrams and their contributions are shown in figure 8 and table 6, respectively. The correspondence

Table 5
Algebraic expressions for $\Gamma_1(J_1J_2 : I_1I_2)$ associated with diagrams of figure 7.

Coupling coefficient	Diagram (figure 7)	Contribution
$\Gamma_1(PR:AB)$	(a_1)	$-t^{RQ}_{BA}(j) = t^{RQ}_{AB}(j)$
	(a_2)	$-\mathbf{P}_{AB} w^R_B(ji)\, t^Q_A(j)$
		$= \mathbf{P}_{AB} w^R_A(ji)\, t^Q_B(j)$
	(a_3)	$\mathbf{P}_{AB} t^P_A(i)\, t^{QR}_{BP}(j)$
	(a_4)	$\mathbf{P}_{AB} t^P_A(i)\, t^Q_B(j)\, t^R_P(j)$
$\Gamma_1(RS:AQ)$	(b_1)	$t^{RS}_{AP}(j)$
	(b_2)	$\mathbf{P}_{RS} w^R_A(ji)\, t^S_P(j)$
	(b_3)	$\mathbf{P}_{RS} t^S_Q(i)\, t^{RQ}_{PA}(j)$
	(b_4)	$\mathbf{P}_{RS} t^S_Q(i)\, t^R_P(j)\, t^Q_A(j)$
$\Gamma_1(RP:AQ)$	(c_1)	$w^R_A(ji)$
	(c_2)	$t^P_A(i)\, t^R_P(j)$
	(c_3)	$-t^R_Q(i)\, t^Q_A(j)$
$\Gamma_1(RS:AB)$	(d_1)	$t^{RSQ}_{ABP}(j)$
	(d_2)	$-\mathbf{P}_{AB} t^Q_A(j)\, t^{RS}_{PB}(j)$
		$= \mathbf{P}_{AB} t^Q_A(j)\, t^{RS}_{BP}(j)$
	(d_3)	$-\mathbf{P}_{RS} t^R_P(j)\, t^{QS}_{AB}(j)$
	(d_4)	$-\mathbf{P}_{RS}\mathbf{P}_{AB} w^R_A(ji)\, t^{QS}_{BP}(j)$
	(d_5)	$-\mathbf{P}_{RS}\mathbf{P}_{AB} w^R_A(ji)\, t^Q_B(j)\, t^S_P(j)$

Table 6
Algebraic expressions for $\Gamma_2(J : I)$ associated with diagrams of figure 8.

Coupling coefficient	Diagram (figure 8)	Contribution
$\Gamma_2(P_1 : A)$	(a_1)	$-t^{Q_1Q_2}_{AP_2}(j)$
	(a_2)	$-\mathbf{P}_{Q_1Q_2} t^{Q_1}_A(j)\, t^{Q_2}_{P_2}(j)$
$\Gamma_2(R : Q_1)$	(b_1)	$t^{RQ_2}_{P_1P_2}(j)$
	(b_2)	$\mathbf{P}_{P_1P_2} t^R_{P_1}(j)\, t^{Q_2}_{P_2}(j)$
$\Gamma_2(P_1 : Q_1)$	(c)	$t^{Q_2}_{P_2}(j)$
$\Gamma_2(R : A)$	(d_1)	$t^{RQ_1Q_2}_{AP_1P_2}$
	(d_2)	$-\mathbf{P}_{P_1P_2}\mathbf{P}_{Q_1Q_2} t^{Q_1}_{P_1}(j)\, t^{Q_2R}_{AP_2}(j)$
	(d_3)	$-\mathbf{P}_{P_1P_2}\mathbf{P}_{Q_1Q_2} t^{Q_1}_{P_1}(j)\, t^{Q_2}_A(j)\, t^R_{P_2}(j)$
	(d_4)	$-\mathbf{P}_{Q_1Q_2} t^{Q_1}_A(j)\, t^{RQ_2}_{P_1P_2}(j)$
	(d_5)	$-\mathbf{P}_{P_1P_2} t^R_{P_1}(j)\, t^{Q_1Q_2}_{AP_2}(j)$

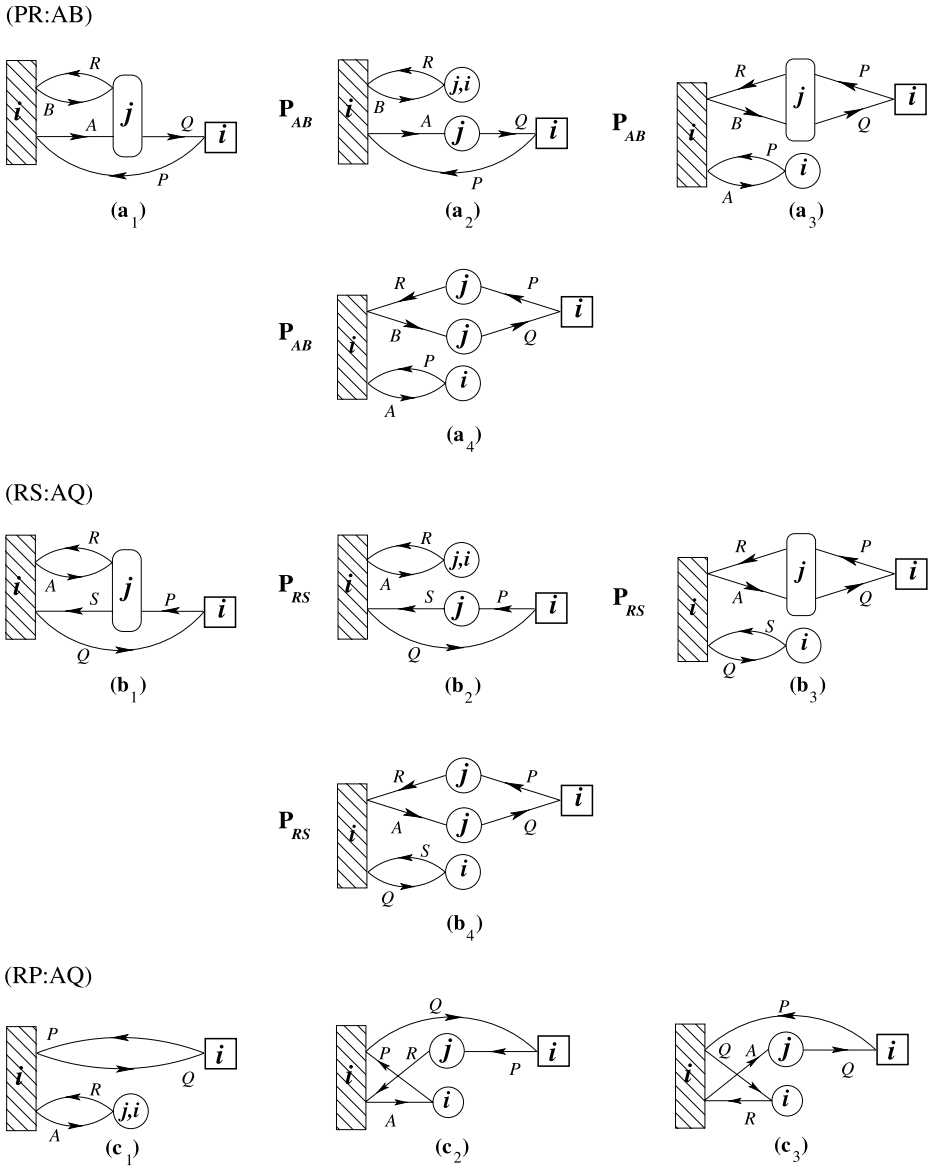

Figure 7. Resulting diagrams for the coupling coefficients $\Gamma_1(J_1J_2 : I_1I_2)$, corresponding to equations (96)–(99) of [13]. Their algebraic equivalents are listed in table 5.

with the algebraically derived expressions given by equations (103)–(106) of [13] is immediately apparent. A similar derivation for doubly-excited bra-configurations is more laborious. For this reason we start with the most laborious case of a pure core-virtual double excitation that leads to the coefficient $\Gamma_2(RS : AB)$. In this case, we shall proceed in a systematic way, starting with nonoriented

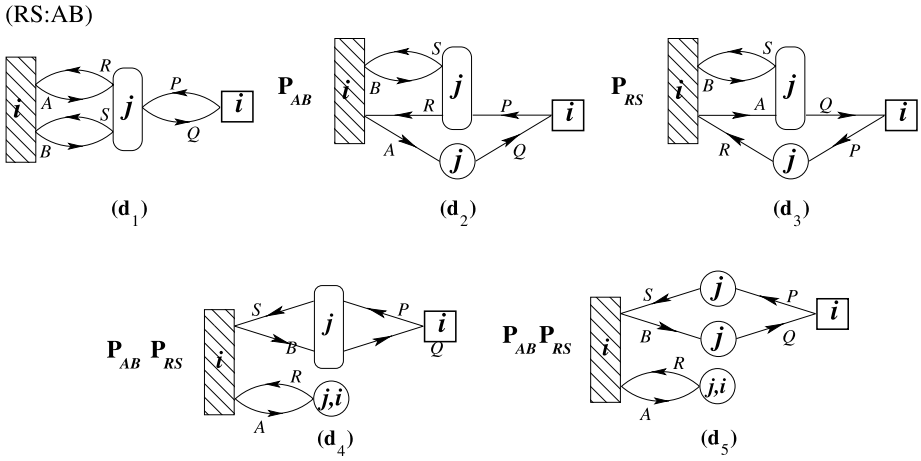

Figure 7. *continued*

Hugenholtz diagrams, as outlined above. For the remaining cases we then present only the resulting diagrams and their algebraic equivalents.

For $\Gamma_2(RS:AB)$ no fermion lines can directly interconnect the bra and ket vertices. In constructing the nonoriented Hugenholtz diagrams we proceed in a systematic way starting with the highest-order single t-vertex and, subsequently, add lower order t-vertices of various types, leading to diagrams shown in figure 9. Introducing, next, the orientation of fermion lines in all possible (allowed) ways, we easily generate the resulting diagrams shown in figure 10, and by applying the above outlined rules we arrive at their algebraic equivalents listed in table 7. In this case, the comparison with an earlier given expression, equation (114) of [13], is not immediately obvious. In fact, by suitably grouping various diagrammatic contributions, as implied in table 7, we can introduce the following intermediates

$$\omega_{IJ}^{KL}(j) = t_{IJ}^{KL}(j) + t_I^K(j)t_J^L(j)\,, \tag{37}$$

$$\xi_{IJ}^{KL}(j) = t_I^K(j)t_J^L(j) - t_I^L(j)t_J^K(j)\,, \tag{38}$$

$$\tau_{IJ}^{KL}(j) = t_{IJ}^{KL}(j) + \xi_{IJ}^{KL}(j)\,, \tag{39}$$

in addition to the quantity $\omega_A^R(ji)$, equation (32), obtaining

$$\begin{aligned}\Gamma_2(RS:AB) = {} & t_{ABP_1P_2}^{RSQ_1Q_2}(j) \\ & + \mathbf{P}_{AB}\left[\mathbf{P}_{RS}w_A^R(ji)\,t_{BP_1P_2}^{SQ_1Q_2}(j) + \mathbf{P}_{Q_1Q_2}t_A^{Q_1}(j)\,t_{BP_1P_2}^{RSQ_2}(j)\right] \\ & + \mathbf{P}_{P_1P_2}\left[\mathbf{P}_{RS}t_{P_1}^R(j)\,t_{ABP_2}^{SQ_1Q_2}(j) + \mathbf{P}_{Q_1Q_2}t_{P_1}^{Q_1}(j)\,t_{ABP_2}^{RSQ_2}(j)\right]\end{aligned}$$

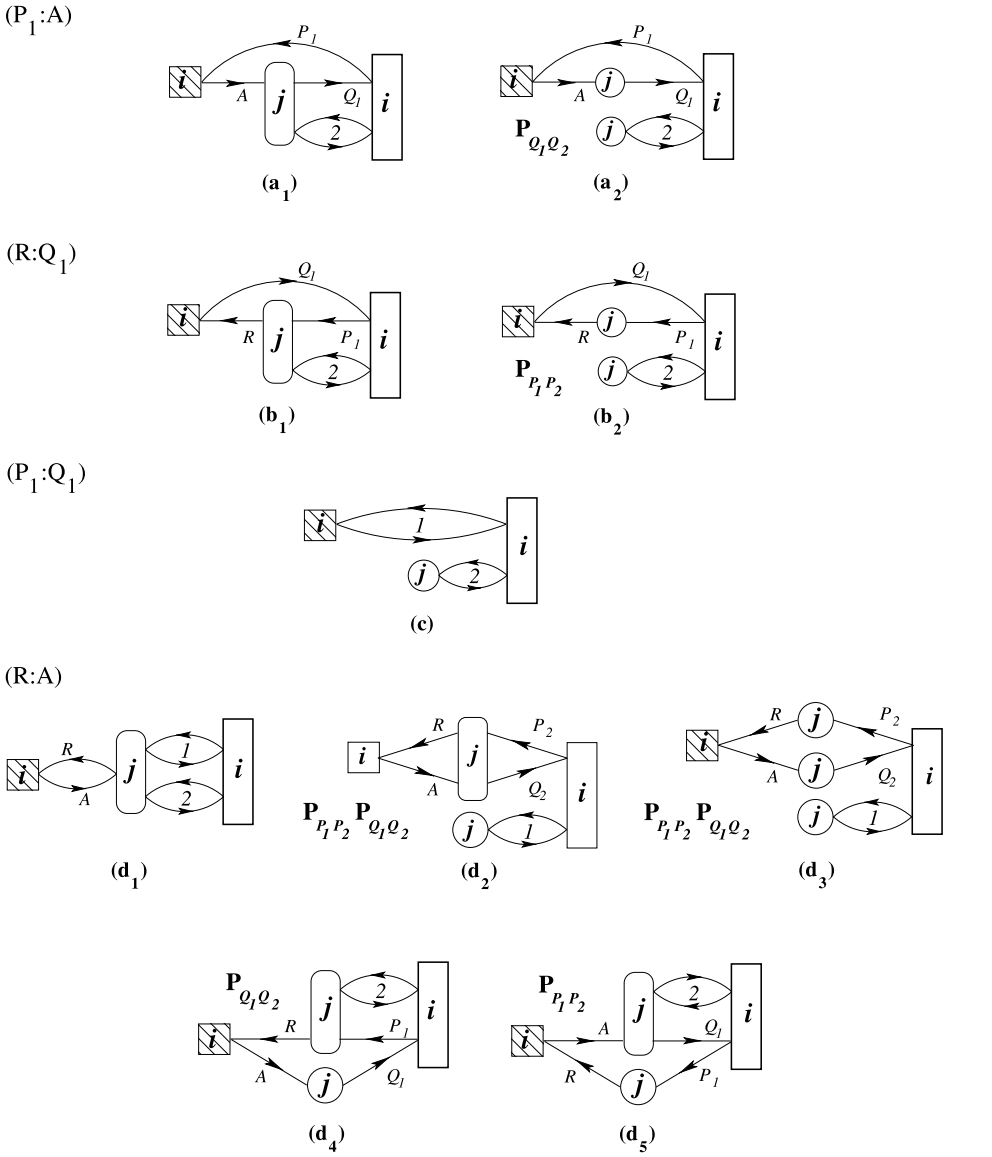

Figure 8. Resulting diagrams for the coupling coefficients $\Gamma_2(J\ :\ I)$, corresponding to equations (103)–(106) of [13]. Their algebraic equivalents are listed in table 6.

$$+\tau^{Q_1Q_2}_{AB}(j)\,\tau^{RS}_{P_1P_2}(j)+\mathbf{P}_{AB}\mathbf{P}_{P_1P_2}\xi^{Q_1Q_2}_{AP_1}(j)\,\xi^{RS}_{BP_2}(j)$$

$$+\mathbf{P}_{AB}\mathbf{P}_{RS}\mathbf{P}_{P_1P_2}\left[\tau^{RQ_1}_{AP_1}(j)\,\tau^{SQ_2}_{BP_2}(j)-\xi^{RQ_1}_{AP_1}(j)\,\xi^{SQ_2}_{BP_2}(j)\right]$$
$$-\mathbf{P}_{AB}\mathbf{P}_{P_1P_2}\tau^{RS}_{P_1B}(j)\,\tau^{Q_1Q_2}_{AP_2}(j)-\mathbf{P}_{RS}\mathbf{P}_{Q_1Q_2}\tau^{RQ_1}_{AB}(j)\,\tau^{SQ_2}_{P_1P_2}(j)$$

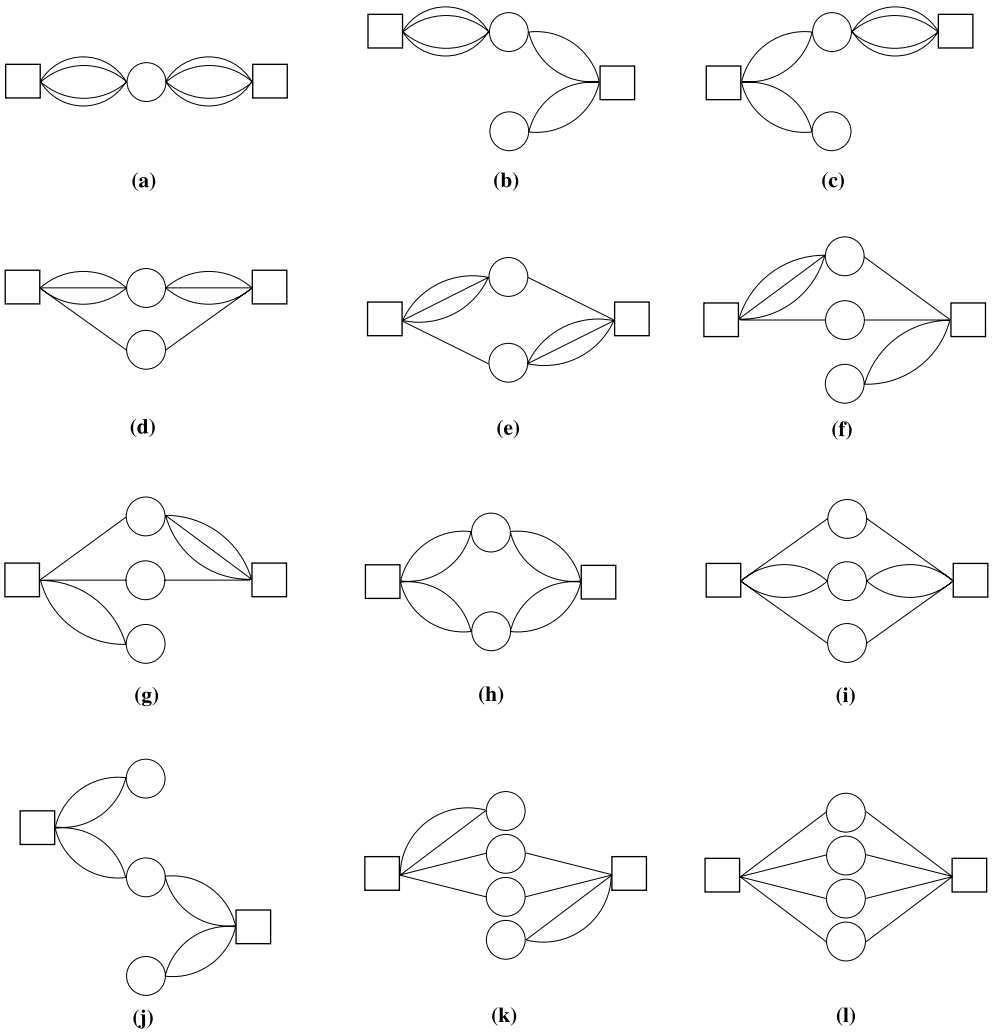

Figure 9. Nonoriented Hugenholtz diagrams for the coupling coefficient $\Gamma_2(RS:AB)$.

$$+\mathbf{P}_{AB}\mathbf{P}_{RS}\left\{t_A^R(i)\left[\mathbf{P}_{P_1P_2}t_{P_1}^S(j)\,t_{BP_2}^{Q_1Q_2}(j)+\mathbf{P}_{Q_1Q_2}t_B^{Q_1}(j)\,t_{P_1P_2}^{SQ_2}(j)\right.\right.$$
$$\left.\left.+\mathbf{P}_{P_1P_2}\mathbf{P}_{Q_1Q_2}t_{P_1}^{Q_1}(j)\,\omega_{P_2B}^{SQ_2}(j)\right]\right\}. \tag{40}$$

The reader can easily verify the equivalence of both expressions, equations (40) and (114) of [13].

For the remaining coupling coefficients $\Gamma_2(J_1J_2 : I_1I_2)$, the resulting diagrams are listed in figures 11 and 12(a)–12(c), and their algebraic evaluation is given in tables 8 and 9(a)–9(c), respectively. More compact expressions

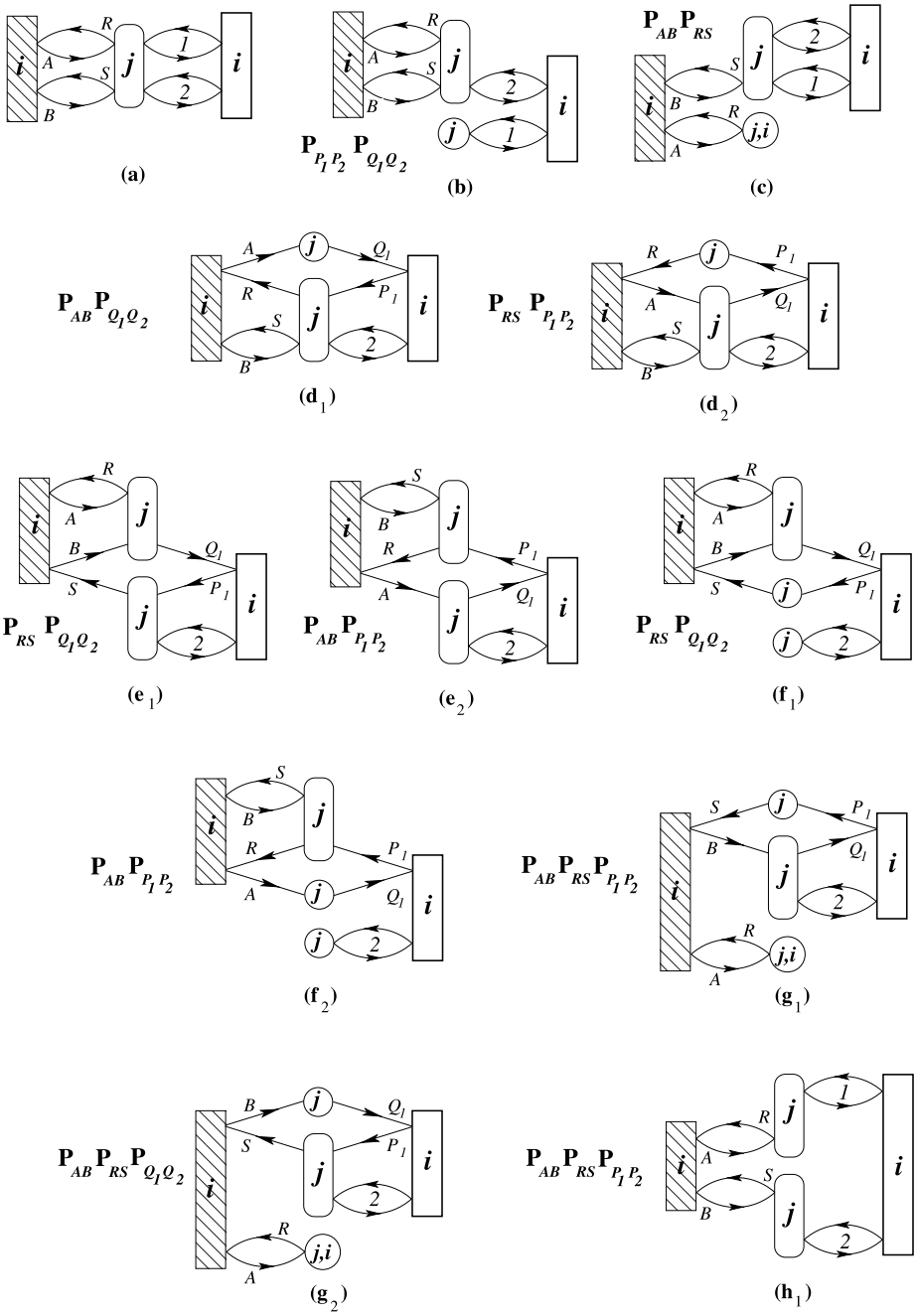

Figure 10. Resulting diagrams for the coupling coefficient $\Gamma_2(RS : AB)$, corresponding to equation (114) of [13]. Their algebraic equivalents are listed in table 7.

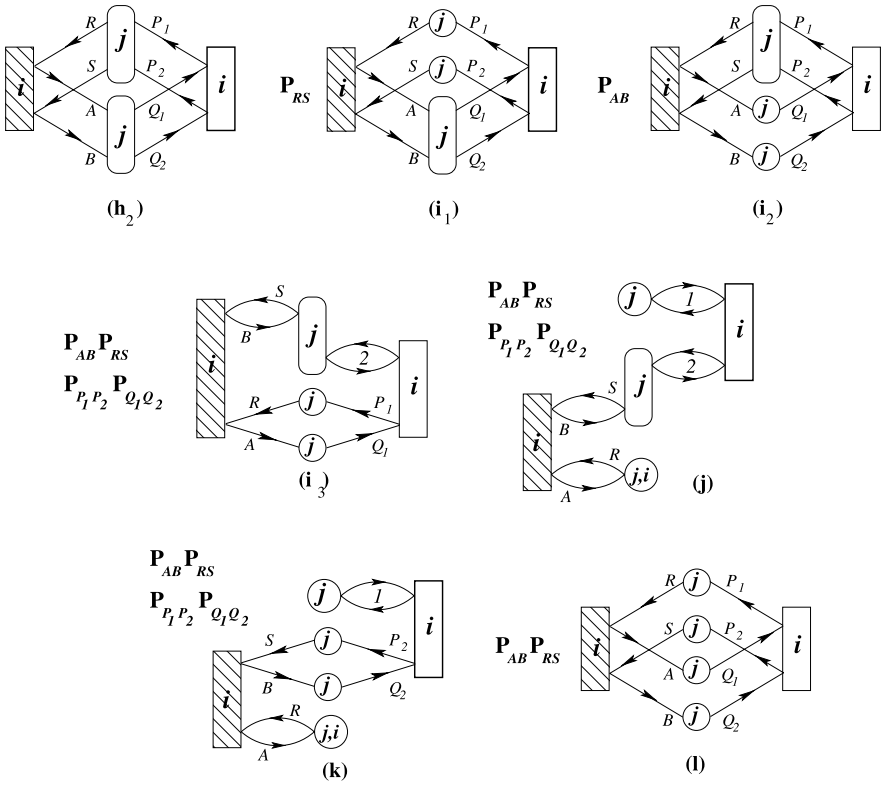

Figure 10. *continued*

for these coefficients, based on our diagrammatic results, can be written as follows:

$$\begin{aligned}\Gamma_2(RP_1:AQ_1) = {} & \tau^{RQ_2}_{AP_2}(j) - t^R_A(i)\, t^{Q_2}_{P_2}(j) + t^{P_1}_A(i)\, \tau^{RQ_2}_{P_1P_2}(j) - t^R_{Q_1}(i)\, \tau^{Q_1Q_2}_{AP_2}(j) \\ & + t^{P_1}_{Q_1}(i) \left\{ -t^{RQ_1Q_2}_{AP_1P_2}(j) + \mathbf{P}_{Q_1Q_2} t^{Q_1}_A(j)\, t^{RQ_2}_{P_1P_2}(j) \right. \\ & \left. + \mathbf{P}_{P_1P_2} \left[t^R_{P_1}(j)\, t^{Q_1Q_2}_{AP_2}(j) + \mathbf{P}_{Q_1Q_2} t^{Q_2}_{P_2}(j)\, \omega^{Q_1R}_{AP_1}(j) \right] \right\}, \end{aligned} \tag{41}$$

$$\begin{aligned}\Gamma_2(RP_1:AB) = {} & -t^{RQ_1Q_2}_{ABP_2}(j) + \mathbf{P}_{AB} t^{P_1}_A(i) \left\{ t^{RQ_1Q_2}_{BP_1P_2}(j) - \mathbf{P}_{Q_1Q_2} t^{Q_1}_B(j)\, \tau^{RQ_2}_{P_1P_2}(j) \right. \\ & \left. - \mathbf{P}_{P_1P_2} \left[t^R_{P_1}(j)\, t^{Q_1Q_2}_{BP_2}(j) - \mathbf{P}_{Q_1Q_2} t^{Q_1}_{P_1}(j)\, t^{RQ_2}_{BP_2}(j) \right] \right\} \\ & + \mathbf{P}_{AB} \mathbf{P}_{Q_1Q_2} t^{Q_2}_A(j)\, t^{Q_1R}_{BP_2}(j) - t^R_{P_2}(j)\, \tau^{Q_1Q_2}_{AB}(j) \\ & - \mathbf{P}_{AB} w^R_A(ji)\, \tau^{Q_1Q_2}_{BP_2}(j) + \mathbf{P}_{Q_1Q_2} t^{Q_2}_{P_2}(j)\, t^{Q_1R}_{AB}(j), \end{aligned} \tag{42}$$

Table 7
Algebraic expressions for the diagrams representing $\Gamma_2(RS:AB)$ of figure 10.

Diagram (figure 10)	Contribution
(a)	$t_{ABP_1P_2}^{RSQ_1Q_2}(j)$
(b)	$\mathbf{P}_{P_1P_2}\mathbf{P}_{Q_1Q_2}t_{P_1}^{Q_1}(j)\,t_{ABP_2}^{RSQ_2}(j)$
(c)	$\mathbf{P}_{AB}\mathbf{P}_{RS}w_A^R(ji)\,t_{BP_1P_2}^{SQ_1Q_2}(j)$
(d_1)	$-\mathbf{P}_{AB}\mathbf{P}_{Q_1Q_2}t_A^{Q_1}(j)\,t_{BP_1P_2}^{SRQ_2}(j)$
(d_2)	$-\mathbf{P}_{RS}\mathbf{P}_{P_1P_2}t_{P_1}^{R}(j)\quad t_{BAP_2}^{SQ_1Q_2}(j)$
(e_1), (f_1)	$-\mathbf{P}_{RS}\mathbf{P}_{Q_1Q_2}t_{AB}^{RQ_1}(j)\,\tau_{P_1P_2}^{SQ_2}(j)$
(e_2), (f_2)	$-\mathbf{P}_{AB}\mathbf{P}_{P_1P_2}t_{P_1B}^{RS}(j)\,\tau_{AP_2}^{Q_1Q_2}(j)$
(g_1)	$-\mathbf{P}_{AB}\mathbf{P}_{RS}\mathbf{P}_{P_1P_2}w_A^R(ji)\,t_{P_1}^{S}(j)\,t_{BP_2}^{Q_1Q_2}(j)$
(g_2)	$-\mathbf{P}_{AB}\mathbf{P}_{RS}\mathbf{P}_{Q_1Q_2}w_A^R(ji)\,t_{B}^{Q_1}(j)\,t_{P_1P_2}^{SQ_2}(j)$
(h_1)	$\mathbf{P}_{AB}\mathbf{P}_{RS}\mathbf{P}_{P_1P_2}t_{AP_1}^{RQ_1}(j)\,t_{BP_2}^{SQ_2}(j)$
(h_2), (i_1), (i_2), (l)	$\tau_{AB}^{Q_1Q_2}(j)\,\tau_{P_1P_2}^{RS}(j)$
(i_3)	$-\mathbf{P}_{AB}\mathbf{P}_{RS}\mathbf{P}_{P_1P_2}\mathbf{P}_{Q_1Q_2}t_{P_1}^{R}(j)\,t_{A}^{Q_1}(j)\,t_{BP_2}^{SQ_2}(j)$
(j)	$\mathbf{P}_{AB}\mathbf{P}_{RS}\mathbf{P}_{P_1P_2}\mathbf{P}_{Q_1Q_2}w_A^R(ji)\,t_{P_1}^{Q_1}(j)\,t_{BP_2}^{SQ_2}(j)$
(k)	$-\mathbf{P}_{AB}\mathbf{P}_{RS}\mathbf{P}_{P_1P_2}\mathbf{P}_{Q_1Q_2}w_A^R(ji)\,t_{P_1}^{Q_1}(j)\,t_{P_2}^{S}(j)\,t_{B}^{Q_2}(j)$

and

$$\begin{aligned}\Gamma_2(RS:AQ_1) = {} & t_{AP_1P_2}^{RSQ_2} + \mathbf{P}_{RS}t_{Q_1}^{R}(i)\left\{t_{AP_1P_2}^{SQ_1Q_2}(j) - \mathbf{P}_{P_1P_2}t_{P_1}^{S}(j)\,\tau_{AP_2}^{Q_1Q_2}(j)\right.\\ & \left. - \mathbf{P}_{Q_1Q_2}\left[t_A^{Q_1}(j)\,t_{P_1P_2}^{SQ_2}(j) - \mathbf{P}_{P_1P_2}t_{P_1}^{Q_1}(j)\,t_{AP_2}^{SQ_2}(j)\right]\right\}\\ & -\mathbf{P}_{RS}\mathbf{P}_{P_1P_2}t_{P_2}^{R}(j)\,t_{P_1A}^{SQ_2}(j) + t_A^{Q_2}(j)\,\tau_{P_1P_2}^{RS}(j)\\ & +\mathbf{P}_{RS}w_A^R(ji)\,\tau_{P_1P_2}^{SQ_2}(j) + \mathbf{P}_{P_1P_2}t_{P_2}^{Q_2}(j)\,t_{AP_1}^{RS}(j)\,. \end{aligned} \tag{43}$$

The equivalence of these formulas, equations (41)–(43), with those given in [13], equtions (111)–(113), respectively, is not difficult to verify when we realize the antisymmetry of Γ coefficients with respect to the spin-orbital interchange, i.e.,

$$\Gamma_2(J_1J_2:I_1I_2) = -\Gamma_2(J_2J_1:I_1I_2) = -\Gamma_2(J_1J_2:I_2I_1) = \Gamma_2(J_2J_1:I_2I_1) \tag{44}$$

and employ definitions (37)–(39).

5. Discussion

We have seen how to generate algebraic expressions for the SU CC coupling coefficients $\Gamma_k(J_1J_2,\ldots,J_m : I_1I_2,\ldots,I_m)$, both in the general form involving

Table 8
Algebraic expressions for the diagrams representing the $\Gamma_2(J_1J_2:I_1I_2)$ coupling coefficients shown in figure 11.

Coupling coefficient	Diagram (figure 11)	Contribution
$\Gamma_2(P_1P_2:AQ_2)$	(a_1)	$-t_A^{Q_1}(j)$
	(a_2)	$-\sum_{\mu=1}^{2} t_A^{P_\mu}(i)\, t_{P_\mu}^{Q_1}(j)$
	(a_3), (a_4)	$\sum_{\mu=1}^{2} t_{Q_2}^{P_\mu}(i)\, \tau_{AP_\mu}^{Q_1Q_2}(j)$
$\Gamma_2(P_1R:Q_1Q_2)$	(b_1)	$t_{P_2}^{R}(j)$
	(b_2)	$-\sum_{\mu=1}^{2} t_{Q_\mu}^{R}(i)\, t_{P_2}^{Q_\mu}(j)$
	(b_3), (b_4)	$-\sum_{\mu=1}^{2} t_{Q_\mu}^{P_1}(i)\, \tau_{P_1P_2}^{Q_\mu R}(j)$
$\Gamma_2(P_1P_2:AB)$	(c_1), (c_2)	$\tau_{AB}^{Q_1Q_2}(j)$
	(c_3), (c_4)	$\mathbf{P}_{AB} \sum_{\mu=1}^{2} t_A^{P_\mu}(i)\, \tau_{P_\mu B}^{Q_1Q_2}(j)$
$\Gamma_2(RS:Q_1Q_2)$	(d_1), (d_2)	$\tau_{P_1P_2}^{RS}(j)$
	(d_3), (d_4)	$-\mathbf{P}_{RS} \sum_{\mu=1}^{2} t_{Q_\mu}^{R}(i)\, \tau_{P_1P_2}^{Q_\mu S}(j)$

Table 9a
Algebraic expressions for the diagrams representing the $\Gamma_2(RP_1:AQ_1)$ coupling coefficients shown in figure 12(a).

Coupling coefficient	Diagram (figure 12)	Contribution
$\Gamma_2(RP_1:AQ_1)$	(a_1)	$t_{AP_2}^{RQ_2}(j)$
	(a_2)	$w_A^R(ji)\, t_{P_2}^{Q_2}(j)$
	(a_3)	$-t_A^{Q_2}(j)\, t_{P_2}^{R}(j)$
		$\Big\} \tau_{AP_2}^{RQ_2}(j) - t_A^R(i)\, t_{P_2}^{Q_2}(j)$
	(a_4)	$-t_{Q_1}^{P_1}(i)\, t_{AP_1P_2}^{RQ_1Q_2}(j)$
	(a_5), (a_6)	$t_A^{P_1}(i)\, \tau_{P_1P_2}^{RQ_2}(j)$
	(a_7), (a_8)	$-t_{Q_1}^{R}(i)\, \tau_{AP_2}^{Q_1Q_2}(j)$
	(a_9)	$t_{Q_1}^{P_1}(i)\, \mathbf{P}_{Q_1Q_2} t_A^{Q_1}(j)\, t_{P_1P_2}^{RQ_2}(j)$
	(a_{10})	$t_{Q_1}^{P_1}(i)\, \mathbf{P}_{P_1P_2} t_{P_1}^{R}(j)\, t_{AP_2}^{Q_1Q_2}(j)$
	(a_{11})	$t_{Q_1}^{P_1}(i)\, \mathbf{P}_{P_1P_2}\mathbf{P}_{Q_1Q_2} t_{P_2}^{Q_2}(j)\, t_{AP_1}^{Q_1R}(j)$
	(a_{12})	$t_{Q_1}^{P_1}(i)\, \mathbf{P}_{P_1P_2}\mathbf{P}_{Q_1Q_2} t_A^{Q_1}(j)\, t_{P_1}^{R}(j)\, t_{P_2}^{Q_2}(j)$

the antisymmetrized CI-type τ-vertices or coefficients and in the explicit form in terms of the CC-type t-vertices or amplitudes, by relying on the diagrammatic technique. Let us now see the connection between these two schemes by considering the transition from the general expressions of the former kind to

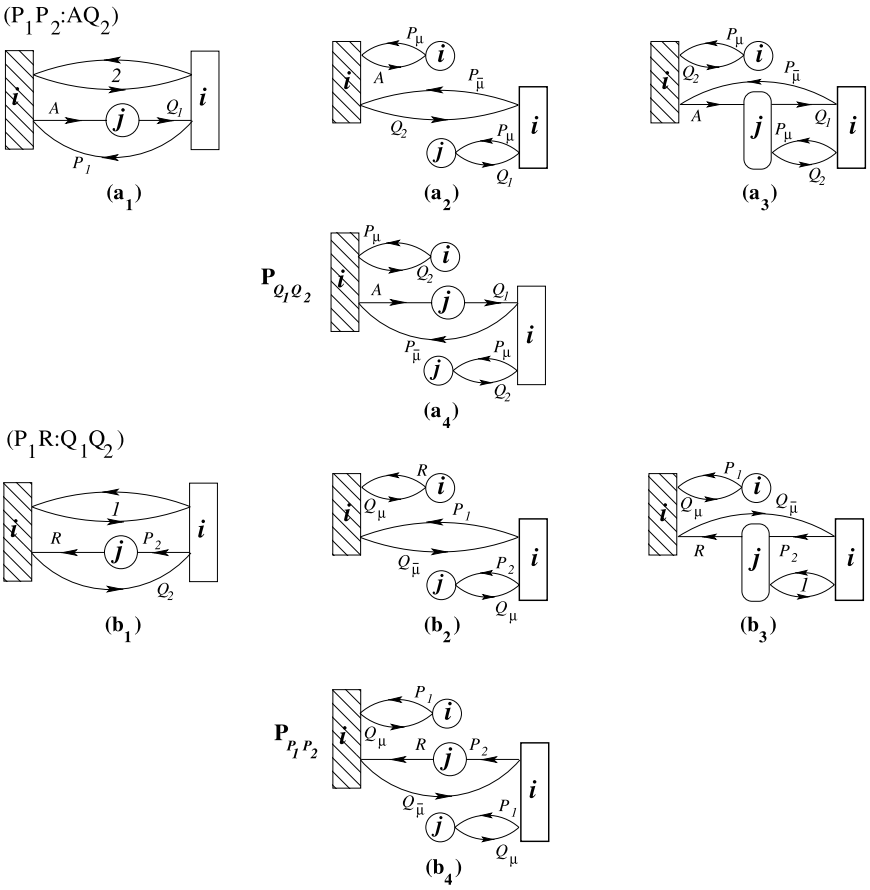

Figure 11. Resulting diagrams for the coupling coefficients $\Gamma_2(J_1J_2:I_1I_2)$, corresponding to equations (107)–(110) of [13]. Note that in the first case we label the MSOs by $(P_1P_2 : AQ_2)$ rather than with $(P_1P_2 : AQ_1)$ as done in [13] in order to achieve the hole-particle symmetry of our diagrams with the case $(P_1R : Q_1Q_2)$. We also define $\overline{\mu} = 3-\mu$ with $\mu = 1, 2$, wherever applicable. The algebraic equivalents are given in table 8.

the explicit formulas in terms of the cluster amplitudes, and let us analyze it in some detail showing how the disconnected terms, which vanish in view of the C-conditions, are automatically eliminated when only connected diagrams are taken into account.

Let us consider the case of the $\Gamma_2(RS:AB)$ coefficient, equation (40) (cf. also equation (85), $k = 2$ and equation (114) of [13]). For $k = 2$, equation (85) of [13] takes the form

$$\Gamma_2(RS:AB) = \tau^{RSQ_1Q_2}_{ABP_1P_2}(j) - \mathbf{P}_{AB}\mathbf{P}_{RS}t^R_A(i)\,\tau^{SQ_1Q_2}_{BP_1P_2}(j)\,. \tag{45}$$

Consider first the last term on the RHS of equation (45), which corresponds to those terms in equation (40) (or in equation (114) of [13]) that involve

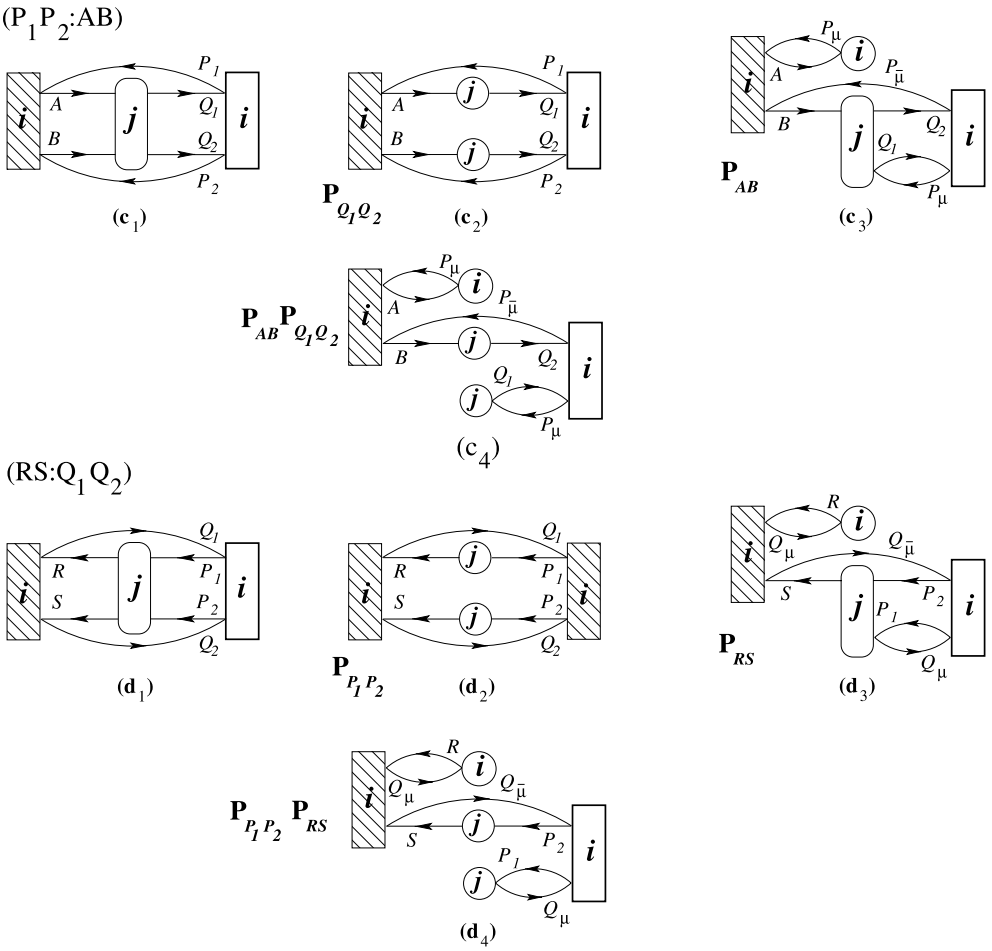

Figure 11. *continued*

the $t(i)$ vertex or amplitude. For the τ coefficient that characterizes this term we easily find that (in all terms we drop the argument j for simplicity's sake)

$$\begin{aligned}\tau^{SQ_1Q_2}_{BP_1P_2} = {} & t^{SQ_1Q_2}_{BP_1P_2} + \underline{t^S_B t^{Q_1Q_2}_{P_1P_2}} - t^S_{P_1} t^{Q_1Q_2}_{BP_2} + t^S_{P_2} t^{Q_1Q_2}_{BP_1} \\ & - t^{Q_1}_B t^{SQ_2}_{P_1P_2} + t^{Q_1}_{P_1} t^{SQ_2}_{BP_2} - t^{Q_1}_{P_2} t^{SQ_2}_{BP_1} \\ & + t^{Q_2}_B t^{SQ_1}_{P_1P_2} - t^{Q_2}_{P_1} t^{SQ_1}_{BP_2} + t^{Q_2}_{P_2} t^{SQ_1}_{BP_1} \\ & + \underline{t^S_B \left(t^{Q_1}_{P_1} t^{Q_2}_{P_2} - t^{Q_1}_{P_2} t^{Q_2}_{P_1} \right)} \\ & - t^S_{P_1} \left(t^{Q_1}_B t^{Q_2}_{P_2} - t^{Q_1}_{P_2} t^{Q_2}_B \right) \\ & + t^S_{P_2} \left(t^{Q_1}_B t^{Q_2}_{P_1} - t^{Q_1}_{P_1} t^{Q_2}_B \right) , \end{aligned} \tag{46}$$

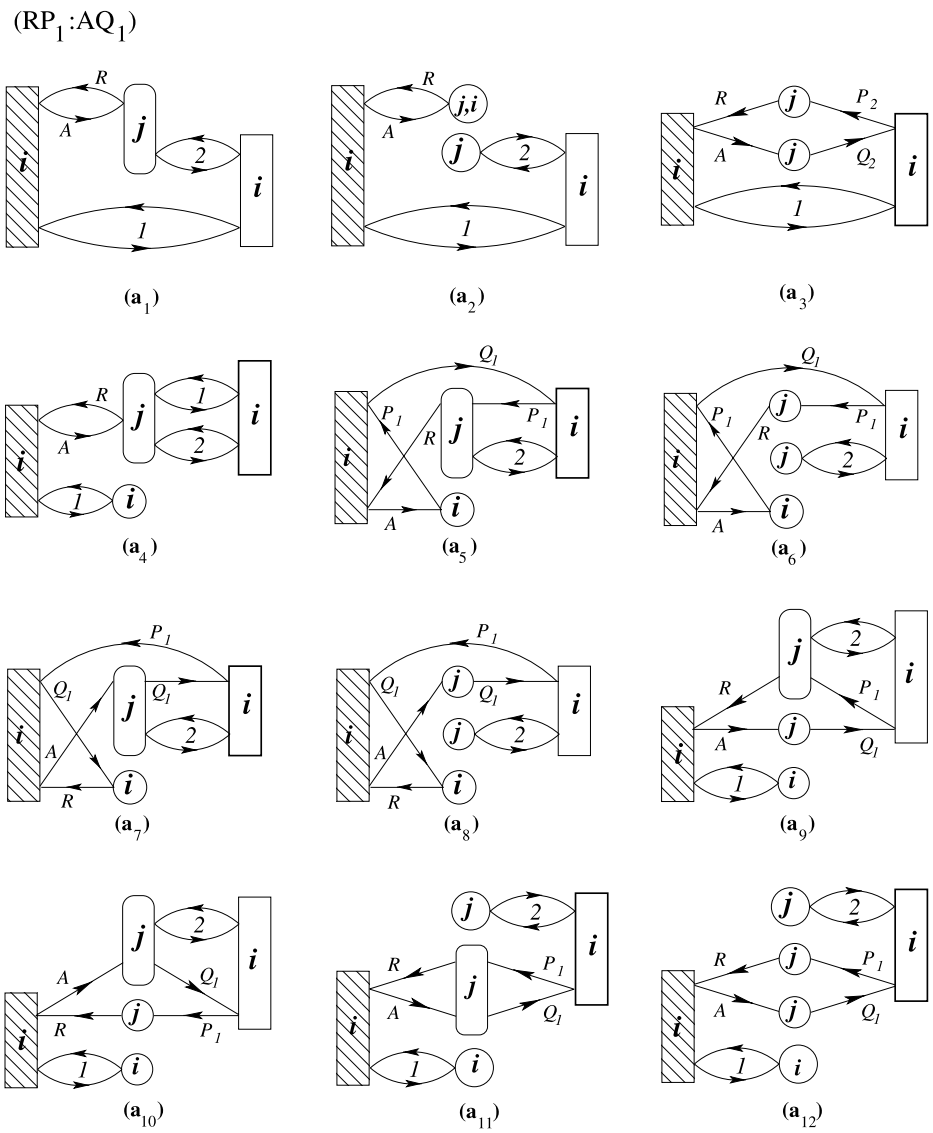

Figure 12a. Resulting diagrams for the coupling coefficient $\Gamma_2(RP_1{:}AQ_1)$, corresponding to equation (111) of [13]. The algebraic equivalents are given in table 9a. For simplicity's sake, we do not explicitly indicate the relevant permutation operators $\mathbf{P}_{P_1P_2}$ and $\mathbf{P}_{Q_1Q_2}$ in the figure, since these are easily determined from the corresponding Hugenholtz diagrams (by identifying the relevant nonequivalent fermion lines) and are included in the algebraic expressions in table 9a.

thus involving one T_3 term, $3^2 = 9$ T_1T_2 terms, and $3! = 6$ terms of the $\frac{1}{3!}T_1^3$ type.

Substitute, next, the above given expression, equation (46), for $\tau^{SQ_1Q_2}_{BP_1P_2}(j)$ into the second term on the RHS of equation (45) and compare the result with the

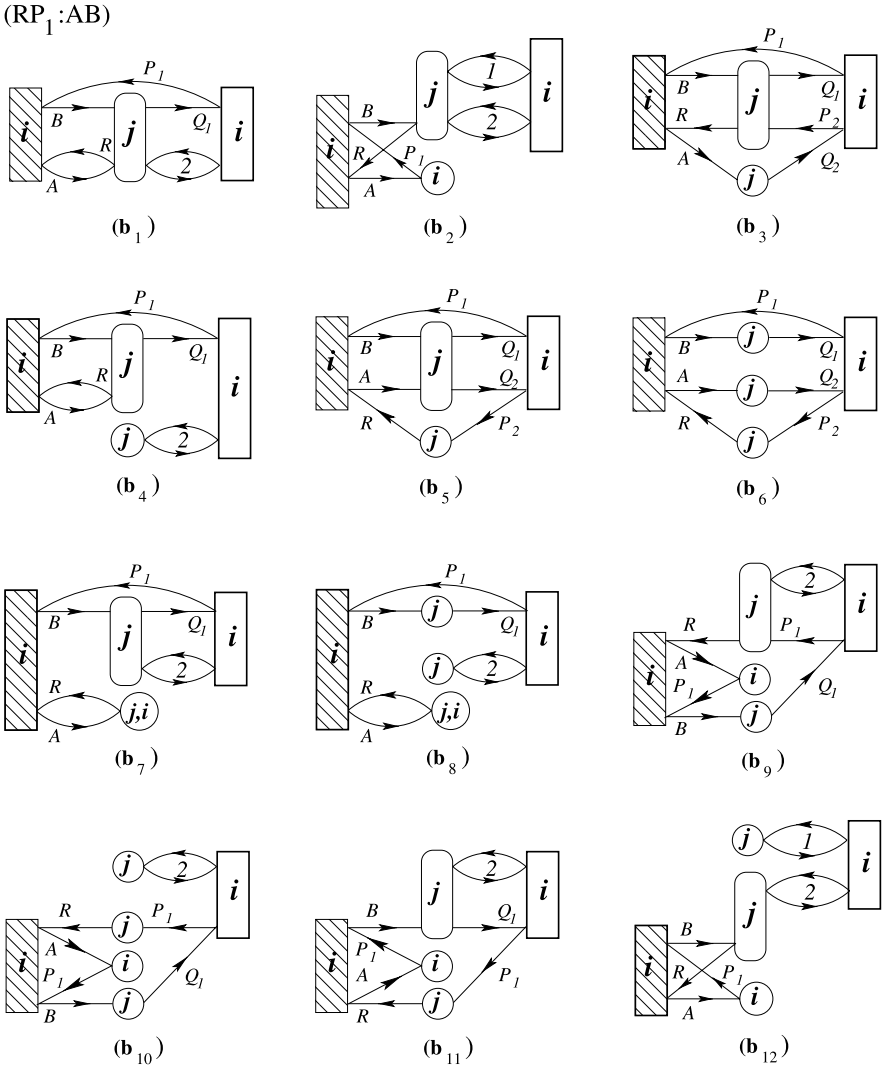

Figure 12b. Resulting diagrams for the coupling coefficient $\Gamma_2(RP_1 : AB)$, corresponding to equation (112) of [13]. The algebraic equivalents are given in table 9b. For simplicity's sake, we do not explicitly indicate the relevant permutation operators $\mathbf{P}_{AB}$, $\mathbf{P}_{P_1P_2}$, and $\mathbf{P}_{Q_1Q_2}$ in the figure, since these are easily determined from the corresponding Hugenholtz diagrams (by identifying the relevant nonequivalent fermion lines) and are included in the algebraic expressions in table 9b.

corresponding terms of this type in equation (40) (namely those involving the amplitude $t_A^R(i)$). We easily find that we can recover all the terms of this type appearing in equation (40) using the terms of equation (46) that are not underlined. Thus, the second term on the RHS of equation (45) involves the additional terms

$$\mathbf{P}_{AB}\mathbf{P}_{RS}t_A^R(i)\,t_B^S(j)\left[t_{P_1P_2}^{Q_1Q_2}(j)+t_{P_1}^{Q_1}t_{P_2}^{Q_2}-t_{P_2}^{Q_1}t_{P_1}^{Q_2}\right]=\mathbf{P}_{AB}\mathbf{P}_{RS}t_A^R(i)\,t_B^S(j)\,\tau_{P_1P_2}^{Q_1Q_2}(j)\,. \tag{47}$$

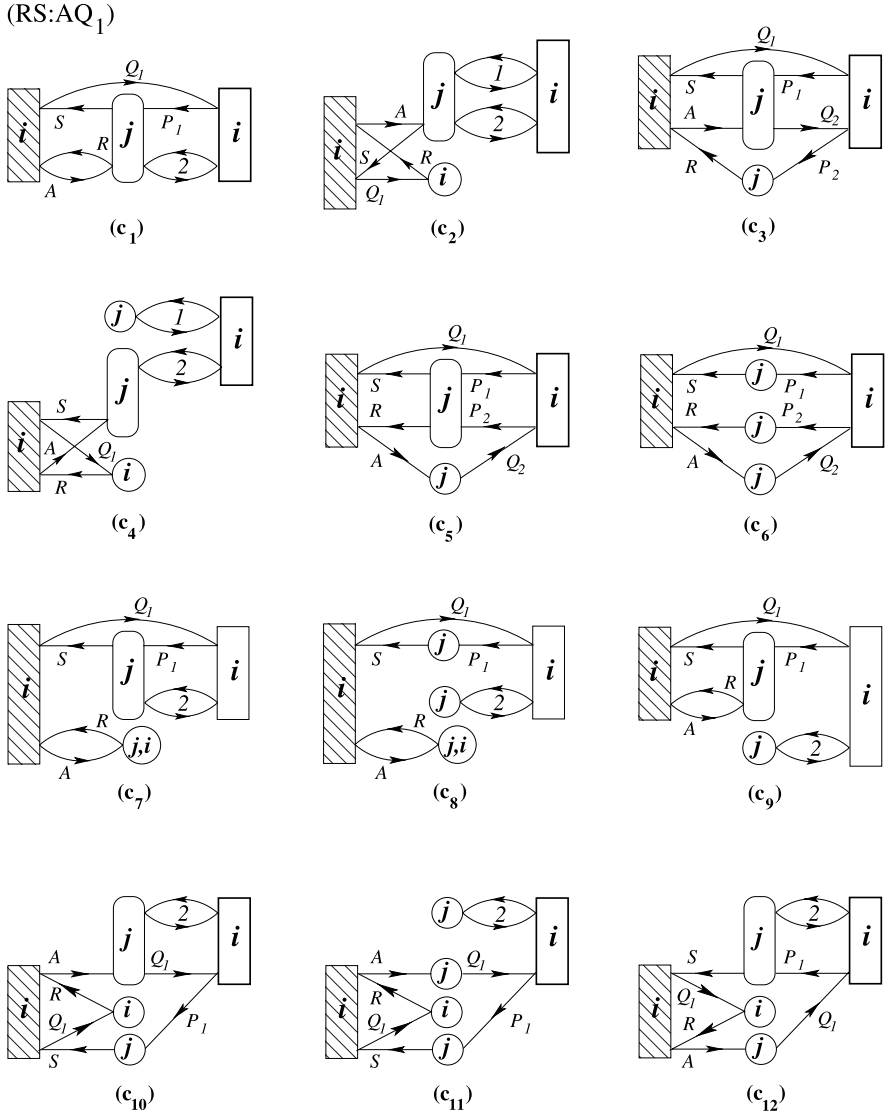

Figure 12c. Resulting diagrams for the coupling coefficient $\Gamma_2(RS : AQ_1)$, corresponding to equation (113) of [13]. The algebraic equivalents are given in table 9c. For simplicity's sake, we do not explicitly indicate the relevant permutation operators $\mathbf{P}_{RS}$, $\mathbf{P}_{P_1P_2}$, and $\mathbf{P}_{Q_1Q_2}$ in the figure, since these are easily determined from the corresponding Hugenholtz diagrams (by identifying the relevant nonequivalent fermion lines) and are included in the algebraic expressions in table 9c.

However, these terms vanish in view of the C-condition

$$\tau^{Q_1Q_2}_{P_1P_2}(j) = 0\,, \tag{48}$$

Table 9b
Algebraic expressions for the diagrams representing the $\Gamma_2(RP_1:AB)$ coupling coefficients shown in figure 12(b).

Coupling coefficient	Diagram (figure 12)	Contribution
$\Gamma_2(RP_1:AB)$	(b_1)	$-t_{AB\,P_2}^{RQ_1Q_2}(j)$
	(b_2)	$\mathbf{P}_{AB}t_A^{P_1}(i)\,t_{B\,P_1P_2}^{RQ_1Q_2}(j)$
	(b_3)	$\mathbf{P}_{AB}\mathbf{P}_{Q_1Q_2}t_A^{Q_2}(j)\,t_{B\,P_2}^{Q_1R}(j)$
	(b_4)	$-\mathbf{P}_{Q_1Q_2}t_{P_2}^{Q_2}(j)\,t_{A\,B}^{RQ_1}(j)$
	(b_5), (b_6)	$t_{P_2}^{R}(j)\,\tau_{B\,A}^{Q_1Q_2}(j)$
	(b_7), (b_8)	$-\mathbf{P}_{AB}w_A^R(ji)\,\tau_{B\,P_2}^{Q_1Q_2}(j)$
	(b_9), (b_{10})	$-\mathbf{P}_{AB}\mathbf{P}_{Q_1Q_2}t_A^{P_1}(i)\,t_B^{Q_1}(j)\,\tau_{P_1P_2}^{RQ_2}(j)$
	(b_{11})	$-\mathbf{P}_{AB}t_A^{P_1}(i)\mathbf{P}_{P_1P_2}t_{P_1}^{R}(j)\,t_{B\,P_2}^{Q_1Q_2}(j)$
	(b_{12})	$\mathbf{P}_{AB}\mathbf{P}_{Q_1Q_2}t_A^{P_1}(i)\mathbf{P}_{P_1P_2}t_{P_1}^{Q_1}(j)\,t_{B\,P_2}^{RQ_2}(j)$

Table 9c
Algebraic expressions for the diagrams representing the $\Gamma_2(RS:AQ_1)$ coupling coefficients shown in figure 12(c).

Coupling coefficient	Diagram (figure 12)	Contribution
$\Gamma_2(RS:AQ_1)$	(c_1)	$t_{A\,P_1P_2}^{RSQ_2}$
	(c_2)	$\mathbf{P}_{RS}t_{Q_1}^{R}(i)\,t_{A\,P_1P_2}^{SQ_1Q_2}(j)$
	(c_3)	$-\mathbf{P}_{RS}\mathbf{P}_{P_1P_2}t_{P_2}^{R}(j)\,t_{P_1A}^{SQ_2}(j)$
	(c_4)	$\mathbf{P}_{RS}\mathbf{P}_{P_1P_2}t_{Q_1}^{R}(i)\mathbf{P}_{Q_1Q_2}t_{P_1}^{Q_1}(j)\,t_{A\,P_2}^{SQ_2}(j)$
	(c_5), (c_6)	$-t_A^{Q_2}(j)\,\tau_{P_2P_1}^{RS}(j)=t_A^{Q_2}(j)\,\tau_{P_1P_2}^{RS}(j)$
	(c_7), (c_8)	$\mathbf{P}_{RS}w_A^R(ji)\,\tau_{P_1P_2}^{SQ_2}(j)$
	(c_9)	$\mathbf{P}_{P_1P_2}t_{P_2}^{Q_2}(j)\,t_{A\,P_1}^{RS}(j)$
	(c_{10}), (c_{11})	$-\mathbf{P}_{RS}\mathbf{P}_{P_1P_2}t_{Q_1}^{R}(i)\,t_{P_1}^{S}(j)\,\tau_{A\,P_2}^{Q_1Q_2}(j)$
	(c_{12})	$-\mathbf{P}_{RS}t_{Q_1}^{R}(i)\,\mathbf{P}_{Q_1Q_2}t_A^{Q_1}(j)\,t_{P_1P_2}^{SQ_2}(j)$

since $G_{P_1P_2}^{Q_1Q_2}(j)$ represents an internal excitation in view of equations (35) and (36). The diagrammatic representation of these terms, equation (47), is shown in figure 13.

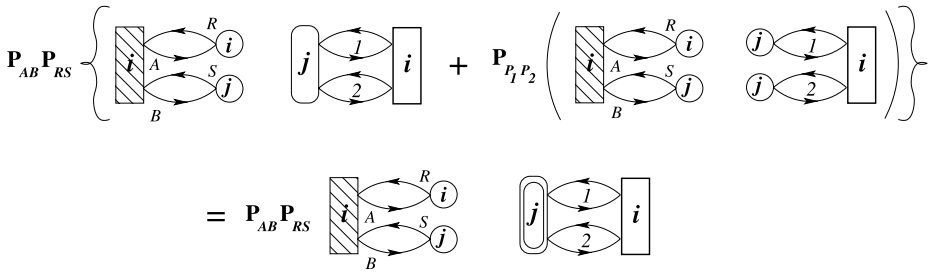

Figure 13. Resulting diagrams representing the disconnected terms (47).

Similarly we can handle the first term on the RHS of equation (45), which is given by $\tau^{RSQ_1Q_2}_{ABP_1P_2}(j)$. Dropping again the argument j in all the amplitudes for simplicity's sake, we can write

$$
\begin{aligned}
\tau^{RSQ_1Q_2}_{ABP_1P_2} &= t^{RSQ_1Q_2}_{ABP_1P_2} \\
&+ \mathbf{P}_{AB}\left[\mathbf{P}_{RS}t^{R}_{A}\,t^{SQ_1Q_2}_{BP_1P_2} + \mathbf{P}_{Q_1Q_2}t^{Q_1}_{A}\,t^{RSQ_2}_{BP_1P_2}\right] \\
&+ \mathbf{P}_{P_1P_2}\left[\mathbf{P}_{RS}t^{R}_{P_1}t^{SQ_1Q_2}_{ABP_2} + \mathbf{P}_{Q_1Q_2}t^{Q_1}_{P_1}t^{RSQ_2}_{ABP_2}\right] \\
&+ \underline{t^{RS}_{AB}\,t^{Q_1Q_2}_{P_1P_2}} + t^{RS}_{P_1P_2}t^{Q_1Q_2}_{AB} \\
&+ \mathbf{P}_{AB}\mathbf{P}_{P_1P_2}\left[\mathbf{P}_{RS}t^{RQ_1}_{AP_1}t^{SQ_2}_{BP_2} - t^{RS}_{P_1B}t^{Q_1Q_2}_{AP_2}\right] \\
&- \mathbf{P}_{RS}\mathbf{P}_{Q_1Q_2}t^{RQ_1}_{AB}\,t^{SQ_2}_{P_1P_2} \\
&+ \mathbf{P}_{AB}\left[\underline{t^{R}_{A}\,t^{S}_{B}\,t^{Q_1Q_2}_{P_1P_2}} + t^{Q_1}_{A}t^{Q_2}_{B}t^{RS}_{P_1P_2}\right] \\
&+ \mathbf{P}_{P_1P_2}\left[\underline{t^{Q_1}_{P_1}t^{Q_2}_{P_2}t^{RS}_{AB}} + t^{R}_{P_1}t^{S}_{P_2}t^{Q_1Q_2}_{AB}\right] \\
&- \mathbf{P}_{AB}\mathbf{P}_{RS}\mathbf{P}_{P_1P_2}\mathbf{P}_{Q_1Q_2}\left(t^{R}_{P_1}t^{Q_1}_{A} - t^{R}_{A}\,t^{Q_1}_{P_1}\right)t^{SQ_2}_{BP_2} \\
&+ \mathbf{P}_{AB}\mathbf{P}_{P_1P_2}\left[\mathbf{P}_{Q_1Q_2}t^{Q_1}_{P_1}t^{Q_2}_{A}t^{RS}_{BP_2} + \mathbf{P}_{RS}t^{R}_{P_1}t^{S}_{A}\,t^{Q_1Q_2}_{BP_2}\right] \\
&- \mathbf{P}_{RS}\mathbf{P}_{Q_1Q_2}\left[\mathbf{P}_{P_1P_2}t^{R}_{P_1}t^{Q_1}_{P_2}t^{SQ_2}_{AB} + \mathbf{P}_{AB}t^{R}_{A}\,t^{Q_1}_{B}t^{SQ_2}_{P_1P_2}\right] \\
&+ \mathbf{P}_{AB}\mathbf{P}_{P_1P_2}\left[\underline{t^{R}_{A}\,t^{S}_{B}\,t^{Q_1}_{P_1}t^{Q_2}_{P_2}} + t^{R}_{P_1}t^{S}_{P_2}t^{Q_1}_{A}t^{Q_2}_{B} + \mathbf{P}_{RS}\mathbf{P}_{Q_1Q_2}t^{R}_{P_1}t^{S}_{A}\,t^{Q_1}_{B}t^{Q_2}_{P_2}\right] \qquad (49)
\end{aligned}
$$

We thus have one four-body amplitude, $4^2 = 16$ terms of the T_1T_3 type, $\frac{1}{2}\binom{4}{2}^2 = 18$ terms of the $\frac{1}{2}T_2^2$ type, $2\cdot\binom{4}{2}^2 = 72$ terms of the $\frac{1}{2}T_1^2T_2$ type, and $4! = 24$ terms of the $\frac{1}{4!}T_1^4$ type.

We see again that these terms yield the corresponding ones occurring in the expression (40), except for those that are underlined, namely

$$
t^{RS}_{AB}\left(t^{Q_1Q_2}_{P_1P_2} + \mathbf{P}_{P_1P_2}t^{Q_1}_{P_1}t^{Q_2}_{P_2}\right) + \mathbf{P}_{AB}t^{R}_{A}\,t^{S}_{B}\left(t^{Q_1Q_2}_{P_1P_2} + \mathbf{P}_{P_1P_2}t^{Q_1}_{P_1}t^{Q_2}_{P_2}\right)
$$

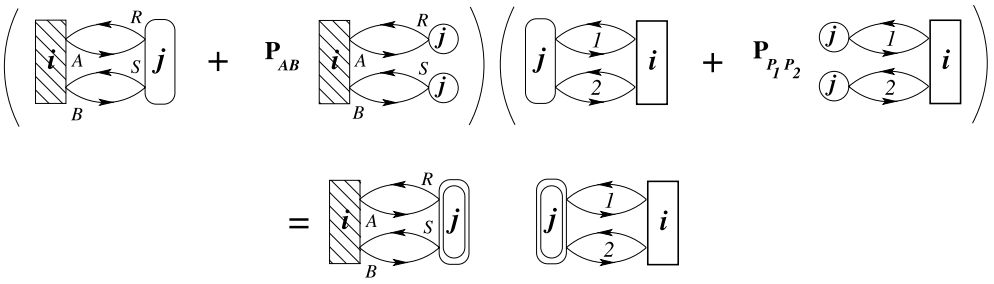

Figure 14. Resulting diagrams representing the disconnected terms (50).

$$
\begin{aligned}
&= \left(t_{AB}^{RS} + \mathbf{P}_{AB} t_A^R t_B^S\right) \left(t_{P_1P_2}^{Q_1Q_2} + \mathbf{P}_{P_1P_2} t_{P_1}^{Q_1} t_{P_2}^{Q_2}\right) \\
&= \tau_{AB}^{RS}\, \tau_{P_1P_2}^{Q_1Q_2}\,, \qquad (50)
\end{aligned}
$$

which vanish in view of the C-condition (48). All these contributions, equation (50), represent again disconnected terms whose diagrammatic representation is shown in figure 14.

We can thus conclude that the diagrammatic approach automatically implements the C-conditions assuming that only connected diagrams are taken into account. An exactly analogous procedure that we have demonstrated for the $\Gamma_2(RS:AB)$ coefficient can be carried out for all other coupling coefficients.

Acknowledgements

Continued support by NSERC (J.P.) is gratefully acknowledged.

References

[1] J. Paldus, Coupled cluster theory, in: *Methods in Computational Molecular Physics*, eds. S. Wilson and G.H.F. Diercksen, NATO ASI Series, Series B: Physics, Vol. 293 (Plenum Press, New York, 1992) pp. 99–194.
[2] J. Paldus, Algebraic approach to coupled cluster theory, in: *Relativistic and Electron Correlation Effects in Molecules and Solids*, ed. G.L. Malli, NATO ASI Series, Series B: Physics, Vol. 318 (Plenum Press, New York, 1994) pp. 207–282.
[3] J. Paldus, Coupled cluster methods, in: *Handbook of Molecular Physics and Quantum Chemistry*, ed. S. Wilson, Vol. 2, Part 3, Chap. 19 (J. Wiley & Sons, Chichester, 2003) pp. 272–313.
[4] I. Lindgren, Int. J. Quantum Chem. S12 (1978) 33.
[5] I. Lindgren and J. Morrison, *Atomic Many-Body Theory* (Springer-Verlag, Berlin, 1982).
[6] I. Lindgren and D. Mukherjee, Phys. Rep. 151 (1987) 93.
[7] D. Mukherjee and S. Pal, Adv. Quantum Chem. 20 (1989) 292.
[8] B. Jeziorski and J. Paldus, J. Chem. Phys. 90 (1989) 2714.
[9] B. Jeziorski and H.J. Monkhorst, Phys. Rev. A 24 (1981), 1668.
[10] J. Čížek, J. Chem. Phys. 45 (1966) 4256.
[11] J. Čížek, Adv. Chem. Phys. 14 (1969) 35.

[12] J. Paldus and X. Li, Adv. Chem. Phys. 110 (1999) 1.
[13] X. Li and J. Paldus, J. Chem. Phys. 119 (2003) 5320.
[14] X. Li and J. Paldus, J. Chem. Phys. 119 (2003) 5334.
[15] X. Li and J. Paldus, J. Chem. Phys. 119 (2003) 5346.
[16] X. Li and J. Paldus, Int. J. Quantum Chem. (in press).
[17] J. Paldus and X. Li, Coll. Czech. Chem. Commun. 69 (2004) 90.
[18] J. Paldus and J. Čížek, Adv. Quantum Chem. 9 (1975) 105.
[19] J. Paldus, Perturbation theory, in: *Atomic, Molecular, and Optical Physics Handbook*, ed. G.W.F. Drake, Chap. 5 (American Institute of Physics, Woodbury, N.Y., 1996) pp. 75–87.
[20] J. Paldus, *Diagrammatic Methods for Many-Fermion Systems* (Lecture Notes, University of Nijmegen, Nijmegen, The Netherlands, 1981).
[21] H. Primas, Separability in many-electron systems, in: *Modern Quantum Chemistry, Istanbul Lectures*, Part II, *Interactions*, ed. O. Sinanoğlu (Academic Press, New York, 1965) pp. 45–74.
[22] J. Paldus, J. Chem. Phys. 67 (1977) 303.
[23] P. Piecuch and J. Paldus, Theor. Chim. Acta 83 (1992) 69.